N O T I C E

THIS DOCUMENT HAS BEEN REPRODUCED FROM MICROFICHE. ALTHOUGH IT IS RECOGNIZED THAT CERTAIN PORTIONS ARE ILLEGIBLE, IT IS BEING RELEASED IN THE INTEREST OF MAKING AVAILABLE AS MUCH INFORMATION AS POSSIBLE

NASA

Technical Memorandum 80719

The Jovian Magnetotail and its Current Sheet

K. W. Behannon
L. F. Burlaga
N. F. Ness

(NASA-TM-80719) THE JOVIAN MAGNETOTAIL AND ITS CURRENT SHEET (NASA) 69 p HC A04/MF A01 CSCL 03B

N81-15923

Unclas

G3/91 12805

OCTOBER 1980

National Aeronautics and
Space Administration

Goddard Space Flight Center
Greenbelt, Maryland 20771

JAN 1981
RECEIVED
NASA STI FACILITY
ACCESS DEPT.

THE JOVIAN MAGNETOTAIL AND ITS CURRENT SHEET

by

K. W. Behannon, L. F. Burlaga and N. F. Ness
Laboratory for Extraterrestrial Physics
NASA/Goddard Space Flight Center
Greenbelt, MD 20771

JUNE 1980

Revised October 1980

SUBMITTED TO: Journal of Geophysical Research

ABSTRACT

Analyses of Voyager magnetic field measurements have extended our understanding of the structural and temporal characteristics of Jupiter's magnetic tail. The magnitude of the magnetic field in the lobes of the tail is found to decrease with Jovicentric distance approximately as $r^{-1.4}$, compared with the power law exponent of -1.7 found for the rate of decrease along the Pioneer 10 outbound trajectory. Voyager observations of magnetic field component variations with Jovicentric distance in the tail do not support the uniform radial plasma out-flow model derived from Pioneer data. Voyager 2 has shown that the azimuthal current sheet which surrounds Jupiter in the inner and middle magnetosphere extends "tailward" (in the anti-Sun direction) to a distance of at least 100 R_J. In the tail this current sheet consists of a plasma sheet and embedded "neutral" sheet. In the region of the tail where the sheet is observed, the variation of the magnetic field as a result of the sheet structure and its 10-hr periodic motion is the dominant variation seen. Studies of both the large-scale configuration of the current sheet viewed as a surface and of the internal structure of the sheet and its orientation indicate that (1) at distances $\gtrsim$ 30 R_J in the tail the sheet is oriented within ±10° of the Jovian equatorial plane, most likely as a result of the solar wind interaction with the Jovian magnetosphere; (2) the surface moves north and south with an amplitude of several R_J with respect to that plane; and (3) at large distances this motion is primarily due to a rocking of the current sheet about the Jupiter-Sun line. A mathematical model that takes the tail geometry into account provides a simpler description of sheet motion in the deep tail than models based on axial symmetry. The plasma sheet in the tail is estimated to have an average thickness $\leq$ 5 R_J.

THE JOVIAN MAGNETOTAIL AND ITS CURRENT SHEET

INTRODUCTION

In situ observations of the magnetic field in the outer Jovian magnetosphere were obtained by the Pioneer 10 and 11 flybys in December, 1973, and December, 1974, respectively (Smith *et al.*, 1974, 1975, 1976). These observations suggested that the outer magnetosphere of Jupiter is dominated by local currents that are confined to a thin ($\sim 2\ R_J$ thick) sheet in which the magnetic field can exhibit large and rapid fluctuations, the magnitude of the field can be very small and the average field in the sheet is southward pointing (Kivelson, 1976; Kivelson *et al.*, 1978). It was concluded from these observations that the field outside the sheet was nearly radial, pointing away from Jupiter above the sheet and toward the planet south of the sheet. The regularity of the Pioneer 10 outbound data outside the current sheet suggested a "magnetotail-like" field (Goertz, 1979), but because Pioneer 10 exited the magnetosphere at a local time (LT) of $\sim$ 0520 and Pioneer 11's outbound pass was near local noon, these spacecraft were unable to establish the existence of a Jovian magnetotail.

The Voyager 1 and 2 flybys of Jupiter in March and July, 1979, respectively, provided an opportunity to observe a magnetospheric tail, since the outbound leg of the Voyager 1 (V1) path through the magnetosphere was near 0400 LT and that of Voyager 2 (V2) was at $\sim$ 0240 LT. The locations of these outbound trajectories in comparison with that of Pioneer 10 (P10) are shown in Figure 1. Preliminary Voyager results have indeed confirmed the presence of a Jovian magnetotail (Ness *et al.*, 1979a, b and c). These results have demonstrated that (1) a fully-developed magnetotail of diameter $\sim$ 300-400 R_J is formed by the interaction of the solar wind with Jupiter's intrinsic magnetic field; (2) the inner magnetosphere's current sheet merges with the tail's "neutral" sheet and plasma sheet at r $\sim$ 30 R_J (R_J = Jovian radius = 71,372 km); (3) distant sheet crossings resemble in appearance crossings of the earth's plasma and neutral sheets, in contrast with the broad, shallow appearance of inner current sheet crossings; and (4) the System III (S3) sheet crossing longitude variation as a function of r is inconsistent with the rigid and non-rigid magnetodisc

models of Smith (1974a,b), Northrop et al., (1974), and Kivelson et al. (1978). Estimates of the magnetic flux in the tail lobes (Ness et al., 1979b) suggested relatively small polar cap "auroral regions", with the northern zone highly eccentric (not encompassing the rotational axis). Analysis of combined magnetic field measurements and low energy charged particle (LECP) data (Lanzerotti et al., 1980) has shown that the energy densities of ions (protons and heavier nuclei) of energies $\sim$ 30 keV are sufficient to provide the diamagnetic depressions in magnetic field strengths observed in crossing the Jovian plasma sheet at $\sim$ 80-120 R_J. Studies by Barbosa et al. (1979) have suggested that protons of energy $\sim$ 10 keV are the dominant constituents of the early morning plasma sheet out to 80 R_J.

In this paper, we present a summary of the results of further analysis of the magnetic field measurements in Jupiter's magnetic tail and in the region of the tail current sheet by both V1 and V2. The Voyager magnetometers have been described in detail by Behannon et al. (1977). The new Voyager magnetotail studies to be discussed include:

(1) a determination of the variation of the average magnetic field magnitude in the lobes of the magnetotail, i.e., outside the plasma sheet, as a function of distance from the planet;

(2) an examination of the variation of $B_\phi/\rho B_\rho$ with distance from Jupiter, where B_ϕ is the azimuthal component of the magnetic field, B_ρ is the radial component, and ρ is the radial distance;

(3) a study of the detailed structure and orientation of the tail current sheet system, including both detailed illustrations of typical sheet crossings and the results of a minimum variance analysis of all V2 tail sheet traversals; and

(4) an investigation of various models which predict the position of the current sheet in the outer Jovian magnetosphere as a function of both time and location; this includes all models previously introduced in the literature, as well as several new models.

The results of these additional studies demonstrate the departure of the Jovian magnetosphere from axial symmetry. In addition, they confirm that the tail current sheet is very thin relative to the scale size of the

magnetosphere, that the distant sheet ($r \gtrsim 30\ R_J$) on the night side tends to lie near the planetary equatorial plane, and that it is constrained to oscillate about the Jupiter-Sun line.

GENERAL MAGNETOTAIL CHARACTERISTICS

The initial *in situ* observations of the Jovian magnetosphere were performed by the Pioneer 10 and 11 spacecraft in 1973 and 1974 (see reviews by Goertz, 1979; Schulz, 1979). Of the four radial traversals of the magnetosphere by these spacecraft, all were on the dayside near local noon, except for P10 which exited the Jovian magnetosphere near the dawn terminator. A major effort in the analysis and interpretation of the data obtained from these spacecraft was directed towards a description of the characteristics of the magnetodisc current sheet. The magnetosphere was viewed as being dominated by this assumed axially symmetric distension of the near equatorial magnetic field containing an enhanced plasma and energetic particle population. On the P10 outbound pass, the distortion of the magnetic field out of the magnetic meridian plane was viewed as a spiraling of the magnetic field due to a radial out-flow of plasma or to waves in the magnetodisc itself.

It was not until the V1 magnetosphere observations at $\sim$ 0400 LT that the existence and characteristics of the Jovian magnetotail were first identified (Ness *et al.*, 1979a,b). These results showed that the magnetic field at increasingly larger radial distances from the planet tended to lie parallel to the equatorial plane of Jupiter and also the ecliptic plane, since the latter is inclined only 3° with respect to the former. More importantly, the azimuthal direction of the field showed an alignment paralleling the magnetopause surface. These data were combined retrospectively with the P10 results and compared to the geometry of the magnetic field in the dawn to midnight sector of Earth's magnetosphere. It then became immediately clear that a large magnetic tail, developed by the solar wind interaction with the planetary magnetic field, must exist at Jupiter. The V2 results added substantially to a validation of this interpretation, showing that at 0300 LT the magnetic field direction clearly indicated the sweeping back of magnetic field lines into the tail

region.

In all the traversals of the Jovian magnetosphere, there has been a persistent and dominant feature of a 10 hr and a sub-10 hr periodicity in the change of polarity of the magnetic field simultaneous with a decrease in the magnitude. This reflects the traversal of the current sheet, both the magnetodisc in the inner magnetosphere as well as the neutral sheet embedded in the magnetic tail of the planet. It is the purpose of this paper to summarize and extend the results and studies of the V1 and V2 data related to the formation of the Jovian magnetic tail and the characteristics of its embedded neutral sheet. The accompanying paper by Connerney et al. (1981) discusses the inner magnetosphere current sheet, that is, the magnetodisc within 30 R_J.

In Figures 2 and 3 are summarized the V1 magnetic field observations outbound at Jupiter through the final magnetopause (MP) traversal. Shown are the 16 min average field magnitude B in nanoteslas (nT), field direction angles λ and δ, and rms deviation of the field. The outbound magnetospheric measurements by V2 are summarized in the same format in Figures 4-6. The initial publication of V2 results (Ness et al., 1979c) was based upon a preliminary and therefore incomplete set of magnetic tail data. Subsequent analysis of the complete data set showed that the V2 spacecraft, following its initial entry into the magnetosheath, was once again located in the magnetic tail of Jupiter for an extended period of time, out to a radial distance of > 250 R_J. Those data are included in Figure 6. For both Voyager spacecraft the field magnitude data show both a general decrease in field strength with increasing distance from the planet and the localized decreases associated with the numerous full or partial current sheet crossings. The latter are also clearly illustrated in the variations in field direction, both in azimuth and inclination, that occur across the sheet. Also of interest are the repeated MP traversals, in particular the multiplicity of V2 crossings (see Lepping et al., 1980).

The geometry of the magnetotail field is more clearly illustrated by means of vector data. Figure 7 shows the projection on the xy plane of subsets of hourly averaged data obtained by the V1 and V2 spacecraft during

their entire transits through the Jovian magnetosphere outbound from periapsis in March and July, 1979, respectively. The model MP corresponds to the surface determined for V2. A logarithmic scale has been used to represent vector field magnitude. The coordinate system used is solar magnetospheric (SM), in which the x-axis points from the planet to the sun and the z-axis lies in a plane defined by the x-axis and the instantaneous position of the magnetic dipole axis. Close to the planet the field is seen to lie in magnetic meridian planes, while farther out the direction is best described as a sweeping back of the field lines so as to parallel the magnetopause surface. In fact, because of the geometry of the spacecraft trajectory, the field direction is found to be almost constant throughout much of the data set from 30 - 200 R_J.

The companion for these data, Figure 8, illustrates the orientation of the magnetic field in the xz and yz projections. This figure clearly illustrates the differences between the tail and the magnetosheath (MS) fields. The high inclination of the magnetic field relative to the xy plane is the most diagnostic feature of the sheath data. Indeed, in the accompanying paper by Lepping et al. (1981), this feature of the MS data is discussed more fully from the view point of the manner in which the interplanetary magnetic field is convectively transported past the Jovian magnetosphere.

Figures 7 and 8 illustrate the periodic traversals of the current sheet and the alternate location of the spacecraft in either the north or south tail lobe; this is identified more readily in Figure 7 by the changing polarity of the magnetic field. In Figure 8 the apparent excursion of the spacecraft in the xz and yz planes is due to the precessional motion of the magnetic dipole axis associated with the planetary rotation and tilt of the dipole axis to the rotation axis and the subsequent rocking of the coordinate axes about the x-axis.

Field Magnitude Dependence on Radial Distance. A study of the magnitude of the magnetic field in the tail lobes has been conducted. The maximum hourly average field magnitude during each 10-hr period, B_{max}, was used to determine the radial variation of the total magnetic field as the

V1 and V2 spacecraft traveled outbound from periapsis. The analysis consisted of a least squares fit of the measured data to a nonlinear power law model $B = Ar^C$ (see Behannon, 1976, Appendix A, for a detailed description of the fitting procedure and the standard error calculation). A similar analysis was performed for comparison purposes using P10 data obtained from the NSSDC. The results are shown in Figure 9.

For clarity of presentation, each of the three data sets have been separated along the abscissa and, as indicated, are to be referenced to radial distance scales which have been similarly shifted. As can be seen, the trends of the respective data sets suggest different rates of lobe field magnitude decrease along the three different outbound trajectories, which had sun-planet-spacecraft angles at the magnetopause of 99°, 115° and 135° for P10, V1, and V2, respectively. An indication of the degree of difference between individual gradients is given by the best-fit power law exponents, which as shown, were -1.70 for P10, -1.50 for V1, and -1.36 for V2. There is no overlap in the standard error ranges on the three exponent values, suggesting that the difference between them is significant. These results are consistent with a deparature from axial symmetry in the radial gradient of the total field outside the current sheet, with a <u>less rapid</u> falloff of B_{max} in the tailward direction than in the dawnside, pretail magnetosphere and also in the predawn tail region, over the same range of radial distance. These falloff rates with r in planetary radii are all steeper than that determined for the earth's magnetotail, where the power law exponent was estimated to lie between -0.3 and -0.7 (Behannon, 1968; Mihalov <u>et al</u>., 1968).

It is seen that there are systematic deviations from the simple power law dependencies. These effects are most noticeable in Figure 9 at and beyond $r = 100\ R_J$ in the V2 and P10 data. V2 observed another, somewhat broader increase in the neighborhood of $r = 50\ R_J$ (see also Figures 4 and 5), as did also the V1 spacecraft. Additional least squares fits were performed on subsets of P10 and V2 data with the obviously enhanced field values omitted, but no significant changes in the parameters of the fits, particularly in the exponent values, were found. Although these features may well signify temporal variations, we cannot uniquely separate temporal

and spatial variations with a single spacecraft. Future studies which both combine these observations with those from plasma and energetic particle experiments on the same spacecraft and compare the measured variations with suitably extrapolated solar wind measurements from the other Voyager spacecraft may make it possible to infer the true nature of such features.

A further interesting result from this study concerns the values of the best-fit power law coefficients (the A values in $B = Ar^C$), which would be the expected B values at 1 R_J if the law were valid in the inner magnetosphere. The respective values obtained for A, together with standard errors, were 13400 ± 3900 nT, 5058 ± 2334 nT, and 3235 ± 519 nT for P10, V1, and V2, respectively. It is seen that the value for P10 is ∿ 4 times that for V2. This is because the average field magnitude measured by P10 inside 60 R_J was higher than was observed by V2 (by 46% at r = 20 R_J), in addition to the generally steeper decrease in B with r seen by P10 throughout the outer magnetosphere. At 20 R_J, a significant fraction (∿ 49%) of the higher average magnitude at P10 can be attributed to its higher magnetic latitude (14° vs 6.7°). This also means, however, that during the average field determination P10 was situated farther from the extended region of influence of the plasma sheet, which also may have contributed to the stronger total field at the spacecraft location.

One can see further in Figure 9 that the P10 data points begin deviating from the best-fit curve planetward of ∿ 40 R_J, whereas the V1 and V2 rates appropriate to the distant magnetosphere in the tailward direction appear to hold in to a distance between 20 and 30 R_J from Jupiter's center. This result supports other evidence for the onset of tail formation at a distance $\lesssim$ 30 R_J.

Relation of Average Lobe Field Strength and Size to Polar Cap Size. We now turn to the question of what can be deduced about the polar cap regions of the Jovian magnetosphere from the observed size of the tail and the tail field strength. As at Earth it can be assumed that the magnetic field in the tail connects to the polar cap (PC), permitting an estimation of the size of the PC region from the observed tail flux. A preliminary estimate based on V1 and P10 data was given by Ness et al. (1979b). Figure

10 shows a comparison of tail field observed near the MP boundary at the observed MP distance by V1, V2 and P10 with calculations from a theoretical model (shown in the Figure) with a PC radius of 8°, 10° and 13°. Since the MP was observed by V2 at widely varying distances, two different points have been plotted corresponding to an average of data near the first encounter with the MP (A) and an average of data near the last two, more distant MP traversals (B). The model calculation assumes the dipole term of the planetary field is responsible for the flux observed in the tail. Under this assumption, we see that the estimate of 10° ± 1° for the angular half-width of the polar cap region is obtained, much smaller than the 18° - 22° found at Earth. If magnetodisc currents are taken into account, then the angular size of the region is estimated to be approximately 16°, nearer that of the earth (Connerney et al., 1981).

Investigation of $B_\phi/\rho B_\rho$ Variation in Magnetotail. In studying the P10 outbound traversal near the dawn terminator, Goertz et al. (1976) suggested that the magnetodisc represented a radial outflow of plasma, or a planetary wind. According to this model, radial outflow would occur beyond some critical distance, the Alfvén radius, which is the distance at which the rotational energy just balances the magnetic energy density. Hill et al. (1974) inferred an Alfvén radius (r_A) of 30 R_J from the Pioneer measurements of Smith et al. (1974). The justification given for the radial outflow conclusion was that the quantity $B_\phi/\rho B_\rho$ was roughly constant throughout the P10 outbound traversal, where B_ϕ is the magnetic dipole coordinate frame azimuthal component of the field, ρ is the radial distance from the dipole axis, and B_ρ is the radial field component. The P10 result was interpreted as being consistent with the spiraling of the field out of meridian planes as a result of the outflowing plasma lagging behind the corotating plasma near the planet (inside $\rho = r_A$).

Although $B_\phi/\rho B_\rho$ is only an indirect indicator, we have investigated this parameter for both V1 and V2. The results are shown in Figures 11 and 12. The data used were hour averages of the System III spherical coordinate azimuthal and radial components and we let $\rho = r$, the radial distance from the center of Jupiter. We do not expect the fact that we used spherical coordinates with $\hat{Z}$ = rotation axis instead of cylindrical

coordinates with $\hat{z}$ = dipole axis to be a serious source of error due to the small angular offset ($\sim 10°$) between the respective polar axes and the generally low latitudes of the Voyager and Pioneer trajectories. The data points are coded according to the region in which the spacecraft was located at the time of the observations in order to delineate any sub-grouping of the results according to physical regime. For comparison, two simple analytical forms have been included: an inverse distance (r^{-1}) and an inverse distance cubed (r^{-3}) variation.

It can be seen that for neither V1 nor V2 is there any clear and unambiguous support for the uniform radial out-flow model derived from the Pioneer data. In the case of both spacecraft, one sees a sharp fallof as a function of r inside r = 30-40 R_J, where the dependence appears to be something like r^{-3}. This steep decrease continues beyond the Alfvén radius estimated for P10. In contrast, the P10 data suggested little variation of the parameter beyond r $\simeq$ 20 R_J (see Figure 2 of Northrop et al., 1974). At larger radial distances, considerable scatter is seen in the Voyager data due to effects of current sheet crossings and time variations in the field. Also for V2 a separation can be seen of data from above and below the current sheet probably due to a relative skew in field orientation across the sheet in System III coordinates. In spite of the scatter in the data, there is evidence for a continued gradually decreasing trend at distances beyond 40 R_J. The observed variation can be quite naturally accounted for as resulting from the sweeping of the magnetospheric field lines out of meridian planes by the solar wind-magnetosphere interaction, as illustrated in Figure 7. In this process the field, which is more nearly radial near the planet, swings around gradually toward being parallel to the MP boundary as the MP is approached simply because the field must conform to the shape of the tail boundary. B_ϕ increases and B_ρ decreases, giving a variation in $B_\phi/\rho B_\rho$ that is less steep than $1/\rho = 1/r$.

Thus, to a distance somewhat beyond the previously estimated Alfvén radius, there is obviously no consistency with a radial out-flow hypothesis. Farther out, there is a continued slow variation as the field components adjust to the changing MP orientation. It is not necessary to invoke radial out-flow to account for the observations. Although the lack

of strong variation beyond 40 R_J makes the test somewhat inconclusive, an interpretation of no radial outflow within the region of analysis is consistent with the evidence from V2 that a component of flow in the corotation direction was observed in the magnetotail out to a distance of $\sim$ 155 R_J, although at greater distances evidence for tailward flow was found nearer the boundary of the tail (Krimigis et al., 1979).

TAIL CURRENT SHEET OBSERVATIONS

An examination of the vector magnetic fields measured by V1 and V2 in the Jovian magnetotail reveals that the dominant variations observed by these spacecraft outbound at Jupiter to a distance of at least 140 R_J were produced by the recurrent passages through the tail current sheet, the motions of which are controlled by the $\sim$ 10-hour planetary rotation period.

We now illustrate some of the general characteristics of the magnetotail current sheet by showing examples of Voyager magnetometer measurements made within the sheet. Figure 10 shows 2.5 hours of V1 9.6 s average magnetic field data taken on March 7, 1979, during a crossing of the tail sheet at a Jovicentric distance of 34 R_J (and a distance of 22 R_J tailward of the dawn-dusk meridian plane). At the bottom is displayed the average field magnitude B with the rms deviation of the field over the 9.6 s averaging period shown immediately above B. Note that the rms deviation is given on a logarithmic scale running from 0.01 to 10 nT. At the top of Figure 13 are shown the heliographic (HG) coordinate longitude and latitude angles λ, δ of the average vector field.

Figure 13 illustrates a classic traversal of a plasma sheet and embedded "neutral" sheet. In the field magnitude variation we see a broad and somewhat unsteady diamagnetic depression produced by the plasma sheet population of protons and ions of heavier nuclei as discussed by Lanzerotti et al. (1980). Note that the depression is asymmetric in that the decrease in B took less time ($\sim$ 55 min) than the subsequent recovery to the unperturbed level ($\sim$ 75 min). At the minimum point of the depression is seen a relatively narrow ($\sim$ 2 min), deeper depression simultaneous with the major variation in field azimuth, λ, and the largest negative deflections

of the δ angle. This narrower depression corresponds to the embedded magnetic "neutral" sheet, within which a minimum average field of $\sim$ 1 nT was observed. As can be seen, the field was unsteady in direction as well as magnitude for most of the extent of the plasma sheet and tended to display an enhanced southward component throughout the plasma sheet region. The rms shows the increase in fluctuation energy within this region, although in this case the increase does not show up as dramatically as it would on a more expanded vertical scale.

Another example, in which the rms enhancement is seen more clearly, is given in Figure 14. Note the change in time scale from Figure 13--there are only 25 minutes of data shown in Figure 14, which illustrates a more complex sheet traversal, as observed by V2 on July 16, 1979, at the Jovicentric distance of 92 R_J. Only approximately 25% of all V1 and V2 sheet crossings resembled the example shown in Figure 13. Distant tail sheet crossings are typically complex, consisting often of a series of partial or full traversals presumably caused by unsteady sheet motions. In this case a series of magnitude decreases were observed, accompanied by first an unsteady rotation of λ and southward deflection of δ, followed by a second, northward excursion of δ together with a second rotation of λ, which finally remained at the azimuthal direction characteristic of the north lobe field. The broadest and deepest depression in B was observed during this second, more rapid directional variation. Because of the unsteady nature of this sheet crossing, the plasma sheet and the "neutral" sheet are indistinguishable in this case.

In order to understand the nature of the higher frequency fluctuations observed within the sheet, data at the highest resolution (60 ms) have been examined for several traversals. A typical example, corresponding to the interval delineated in the B panel of Figure 14 by "60 msec data", is shown in Figure 15. For this 5 min interval we have plotted the field magnitude in the bottom panel and the three Cartesian HG coordinate components of the field, respectively, in the top three panels. No clearly discernible wave trains have been found in the detailed current sheet data examined to date. As illustrated in Figure 15, the fine scale field fluctuations within the sheet are typically quasisinusoidal, with amplitudes on the order of 1 nT

and with "periods" ranging from $\sim$ 5 s to $\sim$ 30 s. In addition to contributions from such fluctuations, there are also equal and at times greater contributions to the enhanced rms within the sheet from the large-scale changes in field magnitude and direction.

Spectral analysis of the magnetic field in the lobes of the magnetotail, i.e., the regions of the tail outside the current sheet, show those regions to be magnetically extremely quiet in general. Spectra computed over frequency ranges from 0.2 Hz to 5 Hz had power spectral densities which were essentially at the magnetometer noise level ($\sim 2 \times 10^{-5}$ nT^2 Hz^{-1} and $\sim 3 \times 10^{-6}$ nT^2/Hz, respectively). These results are consistent with the extremely low cutoff frequencies, corresponding to electron densities of 10^{-5} cm^{-3} or less, found by the plasma wave experiment in the tail lobes (Gurnett *et al.*, 1980).

MINIMUM VARIANCE ANALYSIS OF CURRENT SHEET OBSERVATIONS

Magnetic field data obtained during crossings of the tail current sheet by V2 have been analyzed by means of the method minimum variance analysis as discussed by Sonnerup and Cahill (1967). For each crossing, we analyzed the 9.6 s average vector field values observed within the region in which the field direction changed from that characteristic of one tail lobe to that of the other. A total of 52 traversals were found for which the ratio of intermediate to minimum eigenvalues, E_2/E_3, was greater than 2.0, indicating that the estimated minimum variance direction was well-determined in those cases (Lepping and Behannon, 1980). An important aspect of the Jovian tail sheet crossings for the minimum variance analysis was that the ω-angle was large in all cases used in the study. ω is the angle in the discontinuity plane (the plane normal to the minimum variance direction) between the projected vector fields bounding the current sheet on each side. For this data set, the average value of ω was 149° and the most probable value was 175°.

Examples of the data used and the resulting hodograms are shown in Figure 16 for three of the crossings. The analysis time intervals and corresponding Jovicentric distances are given in each case. The data are

plotted in HG coordinates at the left side of the figure, and the hodograms at the right display data in the eigenvector system, where $\hat{X}$ is in the direction of maximum variation in the field, $\hat{Z}$ is in the minimum variance direction, and $\hat{Y}$ completes the orthogonal set and designates an intermediate variance direction. Thus, the x-y hodograms show the trace of the tip of the field vector as projected onto the plane perpendicular to the direction of minimum variance.

The cases included in Figure 16 illustrate the major types of features seen in the various sheet traversals analyzed. Based on the hodograms, the crossings fall into four general classes within each of which one particular feature is dominant. The types of classes and number/percent of cases of each type are: simple arc (11/21%), hooked arc(s) (17/33%), nearly linear (11/21%) and complex (13/25%). The crossing at the top of Figure 13 illustrates the complex type, in which there is a complicated hodogram trace as a result of significant variability in either the field direction, its magnitude (as in this case), or both. This may be due to an oscillatory motion of the current sheet with respect to the spacecraft.

At the opposite extreme in complexity are the simple arcs, as in the crossing shown in the center panels, and the nearly linear hodogram, which is not illustrated. The nearly linear hodogram is simply a trace in which there is little variation in the $\hat{Y}$ direction but a large variation in the $\hat{X}$ direction; it results from a dip in field magnitude during the variation in direction. A perfectly linear hodogram corresponds to a degenerate minimum variance solution, and near linearity can signal a poorly determined surface normal direction $\hat{n}$, as defined by the minimum variance direction. For large ω-angle discontinuities, a proportionately larger field magnitude decrease is required to produce degeneracy (down to the limit of $B_{n'n} = 0$ for $\omega = 180°$). Also it is possible to approach closer to the degenerate condition and still have a sufficiently well-resolved variance ellipsoid than is possible for smaller ω cases (Lepping and Behannon, 1980). Since most of the tail sheet traversals had associated ω's near 180°, even most of the nearly linear cases observed were considered to have acceptable solutions.

The fourth and most common class of hodograms obtained in this study was the hooked arc class, illustrated in one of its variety of forms in the lower panels of Figure 16. In some of these forms, the hodograms closely resemble those found by Sonnerup in his analysis of MP structures at Earth (Sonnerup, 1976, 1977). In the case of the earth's MP, Sonnerup attributes such hooks on the hodogram trace to an effect suggested by Parker (1967a,b), in which, for the case of plasma flow tangential to the boundary surface, there are field-aligned electron and ion currents as a result of the differential penetration depths of the two species (each penetrates one gyroradius, with $\Delta R_L \approx R_{Li}$ = 50-100 km). The streaming ions penetrate to the innermost edge of the MP, while electrons are stopped further out. At the magnetospheric edge of a crossing the field direction changes while the magnitude remains essentially constant, producing a hook on the hodogram. It is possible that similar effects may be produced as a result of the separate ion and electron populations in the tail current sheet, possibly near the boundary between the sheet and the lobe field. Alternatively, some of these features may simply be due to unsteady motions of the sheet relative to the spacecraft.

In Figures 17 and 18 we summarize the minimum variance analysis results for the 52 "good" crossing cases. Figure 17 shows the distribution of relative normal component magnitudes, i.e., the relative magnitudes $B_z/\langle|\underset{\sim}{B}|\rangle$ of the field components in the minimum variance directions, where in each case B_z is the normal component and $\langle|\underset{\sim}{B}|\rangle$ is the average total field within the portion of the current sheet being analyzed. As can be seen, the mean value was 0.2 and the most probable value was between 0.1 and 0.2. This distribution suggests that there is generally a nonzero field component normal to the tail sheet. Lepping and Behannon (1980) have found through minimum variance error analysis that discontinuity structures with $B_z/\langle|\underset{\sim}{B}|\rangle > 0.3$ can with 95% confidence be assumed to be structures resembling rotational discontinuities or contact surfaces, that is, they have nonzero normal components when allowance is made for errors in estimating the normal directions. Strictly speaking, only 20% of the observed cases fall into that category, but the upper bound of 0.3 on tangential discontinuity-like (zero normal) structures is a conservative one, and the fact that the distribution does not peak at zero supports the

inference of a generally nonzero normal. The majority of the relatively large $B_z/\langle |\underset{\sim}{B}| \rangle$ cases were found in the near-planet region of the tail, consistent with the field having a larger dipole component there.

Figure 18 shows the directional statistics for the normal components in terms of the latitude angle δ_N and longitude angle λ_N of the tip of the normal vector in HG coordinates. Since the minimum variance analysis cannot distinguish between a vector $\hat{n}$ and $-\hat{n}$, we have removed the arbitrariness by forcing all of the normal vectors to lie in the quadrant defined by $90° \leq \lambda \leq 270°$ and by further ignoring the sign of δ_N. Also, we have removed the geometric bias from the δ_N distribution by using intervals of equal solid angle.

The important features of these distributions are (1) that the normals are closely distributed in λ about 90° and 270°, indicating that the normals oscillate primarily in the dawn-dusk meridian plane, with little tendency for pitching or oscillation in the forward (sunward) or tailward directions; and (2) that they also tend to lie preferably in a fan centered on the normal to the HG equatorial plane ($\delta_N = 90°$). This result suggests that the tail current sheet tends to have a mean orientation approximately parallel to the HG equatorial plane (or possibly the Jovigraphic equatorial plane, since the two planes were nearly equal at the time of the Voyager encounters). Motions of the sheet are limited primarily to oscillations about the planet-sun line, with little evidence for rigid north-south motion or bending about an east-west axis.

SHAPE AND MOTIONS OF THE JOVIAN CURRENT SHEET

Knowledge of the geometrical shape and motion of Jupiter's current sheet is of central importance for studies of Jupiter's magnetosphere and the internal structure of the current sheet. For this purpose the current sheet may be regarded as a mathematical surface, and the problem is to determine an accurate representation of this surface. (It is impossible to find a unique representation.) As discussed in the introduction, the literature contains several models of the current sheet surface which have been applied to P10 observations. All of these models have axial symmetry

with respect to Jupiter's rotation axis, i.e., they imply that all observers at a given distance from Jupiter would see the same sequence of current sheet crossings, except for a phase lag, regardless of their longitude (see Figure 19). Observations of current sheet crossings by V1 (Ness et al., 1979a,b), which moved farther tailward than P10, indicated that the axial models of Goertz (1976b), Hill et al. (1974), Smith et al. (1974, 1975), Kivelson et al. (1978) and Northrop et al. (1974) have limited applicability, and it was suggested that the current sheet on the night side is influenced by the formation of a tail as a result of the interaction of the solar wind with Jupiter's magnetosphere (see Figure 19). V2, which moved much farther tailward than V1 (Figure 19), provided further evidence against the early models and for the effects of a tail (Ness et al., 1979c; Bridge et al., 1979). Carbary (1980) has confirmed that the axial models referenced above do not satisfactorily describe the times of the tail current sheet crossings observed by V1 and V2 (or equivalently the system III longitude at the time of a crossing as a function of the distance of the spacecraft from Jupiter); he showed that the model of Eviatar and Ershkovich (1976) gives a $\phi_{III}(r)$ profile that qualitatively resembles the observations, but he did not actually fit the model to the data.

For our analysis, we have used the measured times of the night-side current sheet crossings determined by the magnetometers on both V1 and V2 between $r \sim 20\ R_J$ and $r \sim 80\ R_J$. Beyond 80 R_J the control of sheet position by planetary rotation apparently began to break down. Current sheet crossings were found to be more randomly spaced in location and time, possibly as a result of solar wind variability and its direct influence on the distant tail position and orientation. In order to evaluate and compare various models of the current sheet configuration, a computer program was developed which gives the best fit of those crossings to an assumed surface. We shall discuss results obtained both from the published axial models (and some modifications of them) and from some new models (non-axial models) which describe the effect of a tail configuration more explicitly.

It is convenient to use a fixed orthogonal Cartesian coordinate system

whose origin is at the center of Jupiter, with $\hat{Z}$ along Jupiter's rotation axis, $\hat{X}$ pointing radially away from the sun and $\hat{Y}$ forming a right-hand triad (Figure 19). In this system the vector $\hat{n}$ directed along the magnetic dipole axis is

$$\hat{n} = -\cos\phi \sin\alpha\, \hat{X} - \sin\phi \sin\alpha\, \hat{Y} + \cos\alpha\, \hat{Z}, \qquad (1)$$

where α is the angle between $\hat{n}$ and the rotation axis $\hat{Z}$ ($\alpha \sim 10°$); here $\phi = \phi(t) = \Omega t$, where Ω is the rotation speed of Jupiter; ϕ is the angle between the projection of $\hat{n}$ on the X-Y plane ($\hat{n}_\perp$) and the $-\hat{X}$-axis, measured positive counterclockwise and equal to zero when $\hat{n}_\perp$ points toward the sun. Thus, $\hat{n}$ precesses about the rotation axis with a period equal to Jupiter's rotation period. For the non-axial models that are discussed below, the current sheet surface may be represented by a vector function $\vec{S} = x\,\hat{X} + y\,\hat{Y} + z(x,y)\,\hat{Z}$, or simply by the function $z(x,y)$ which may depend on $\phi(t)$ and other parameters such as scale lengths. We shall consider models with $z(x,y)$ of the form

$$z(x,y)/\tan\alpha = f(x,y)\cos(\phi + \bar{\phi}) + g(x,y)\sin(\phi + \bar{\phi}), \qquad (2)$$

where $\bar{\phi} = \Omega(x - a)/U$ or $\bar{\phi} = \Omega(r - a)/U$ and $r^2 = x^2 + y^2$. When considering axial models, it is convenient to work in a frame rotating with Jupiter. In this case the surface can be described by a function of the form

$$z'(r', \phi)/\tan\alpha = -h(r')\cos(\phi'(t) + \bar{\phi}'(r')), \qquad (3)$$

where $\bar{\phi}' = \Omega(r' - a)/U$. The motivation for the functional forms (2) and (3) will be apparent when the individual models are discussed.

Axial Models. Four types of axial models for Jupiter's current sheet have been discussed in the literature:

i) Rotating Plane. In this model (Van Allen *et al.*, 1974; Goertz, 1976b) it is assumed that the current sheet is an infinite plane coinciding with the plane of Jupiter's magnetic equator (see sketch at bottom of Figure 20). Since the magnetic dipole axis is inclined with

respect to Jupiter's rotation axis, this plane rotates about the rotation axis. Let $\vec{S} = x\,\hat{X} + y\,\hat{Y} + z\,\hat{Z}$ be a vector in the plane of the current sheet; the condition that the current sheet is a plane normal to $\hat{n}$, where $\hat{n}$ is given by (1), is $\vec{S} \cdot \hat{n} = 0$ which gives

$$z/\tan\alpha = x\cos\phi + y\sin\phi \tag{4}$$

for the equation of the rotating plane relative to the fixed frame. Transforming to the rotating frame gives

$$z'/\tan\alpha = -\,r'\cos\phi'. \tag{5}$$

There are no adjustable parameters in this model.

ii) Hinged Plane or Bent Plane. Smith et al. (1974) and Hill et al. (1974) suggested that the current sheet is a rotating plane (5) out to some distance a from Jupiter (the "hinge point") and that beyond the hinge point is represented by

$$z'/\tan\alpha = -a\cos\phi',\ r' \geq a. \tag{6}$$

A single differentiable function which describes the basic features of this model is

$$z'/\tan\alpha = -\,a\tanh(r'/a)\cos\phi'. \tag{7}$$

We refer to this as the bent plane model, since it reduces to a rotating plane for $r' \ll a$ and to planes parallel to $z = 0$ when $r' \gg a$. There is one adjustable parameter in these models, a. Smith (1974) suggested that the bending might be due to centrifugal force, but it is also possible that it is associated with the formation of a tail.

iii) Rotating Plane with Wave. Kivelson et al. (1978) introduced a 2-parameter model which is basically the rotating plane model with a phase lag $\bar{\phi}' = \Omega(r' - a)/U$ for $r' \geq a$, viz.

$$z'/\tan\alpha = -r'\cos[\phi' + \Omega(r'-a)/U] \qquad (8)$$

for $r' \geq a$ and (5) for $r' < a$. They interpret the phase lag as the result of the time that it takes for information to propagate from $r' = a$ to the observer by means of a wave with speed U. The model of Northrop et al., (1975) and Goertz et al. (1976b) gives a surface similar to (8), but they allow the possibility that U might represent a bulk motion.

iv) Bent Plane with Wave. A 2-parameter model which incorporates all of the basic features discussed above was published by Eviatar and Ershkovich (1976). They assume that 1) close to Jupiter the current sheet is a rigid disc given by (5) at distances $r' < a$; 2) beyond the disc the elevation of the surface is bounded, and 3) there is a phase delay corresponding to the propagation of a wave radially away from the disc. Thus, for $r' \geq a$

$$z'/\tan\alpha = -a\cos[\phi' + \Omega(r'-a)/U]. \qquad (9)$$

Their model resembles that of Kivelson et al. (1978) in that a wave is allowed, but it differs in that it restricts the elevation of the current sheet at large distances. A simple differentiable function representing a surface which is nearly equivalent to that considered by Eviatar and Ershkovich is

$$z'/\tan\alpha = -a\tanh(r'/a)\cos[\phi' + \Omega(r'-a)/U]. \qquad (10)$$

We shall also discuss the case where the signal is allowed to originate at $r' = 0$ rather than $r' = a$, viz.,

$$z'/\tan\alpha = -a\tanh(r'/a)\cos[\phi' - \Omega r'/U]. \qquad (11)$$

Note again that the cause of the bending in those models is not specified.

Now let us consider how the axial models described above fit the V1 and V2 observations of the times of the current sheet crossings on the night-side of Jupiter. The model surface predictions of sheet position z'

were fitted to V1 and V2 crossing positions separately. Bear in mind that V2 moved much farther tailward than V1 and in this sense it was more sensitive to effects of a tail configuration. The results are summarized in Table 1. The 0-parameter rotating plane model gives a poor fit to both V1 and V2, viz. F1 = 5.0 and F2 = 4.9, where F1 and F2 are the rms values of the fits to z' for V1 and V2, respectively, in units of R_J. The 1-parameter bent plane model gives a fair fit to V2, but an unsatisfactory fit to V1. The bent plane model (7) gives essentially the same result as the hinged plane model, in which the surface normal changes discontinuously at the edge of the disc. Allowing a wave (8) instead of bending, gives a fair fit to V1 (F1 = 1.9) but an unsatisfactory fit to V2 (F2 = 3.4). The results of the 2-parameter hinged plane with wave model and our bent plane with wave (10) are essentially the same. Those models give a fair fit to V1 (F1 = 2.1) and a good fit to V2 (F2 = 1.2). Our bent plane with wave model (11), which allows the wave to propagate from r' = 0 instead of from r' = a gives a good fit to both V1 and V2, viz. F1 = 1.2 and F2 = 0.9.

Another way of evaluating the axial models is to plot the system III longitude of the spacecraft at the time of a current sheet crossing as a function of the spacecraft distance from the planet and to compare these observations with predictions of $\phi_{III}(r')$ from the models. Figure 21 shows the observations of ϕ_{III} versus r' for the V2 current sheet crossings. Note that there are two sets of points, one for the south to north (S-N) crossings and another for the north to south (N-S) crossings, and one can imagine a curve through each set of points. There are two basic features of these curves: 1) as r' increases, the two curves converge, and 2) there is an asymmetry, $\phi_{III}(r')$ being flatter for the S-N crossings than for the N-S crossings. The first of these features is due to the bounded elevation z_m, of the current sheet, as illustrated by the curves for the bent plane/no wave model shown in Figure 21. As the spacecraft moved away from Jupiter, its distance above the equatorial plane, $z_{S/C}$, increased. When $z_{S/C} < z_m$ the current sheet crossed the spacecraft twice per Jovian rotation--once going northward, and again when it moved southward. The larger $z_{S/C}(r')$ is, the smaller is $z_m - z_{S/C}$ and thus the shorter the interval between S-N and N-S crossings (and correspondingly, the smaller is $\Delta\phi_{III}$). When $z_{S/C} = z_m$, the current sheet "crossed" the spacecraft just

once, giving a single ϕ_{III}.

The second feature of the $\phi_{III}(r')$ curves, the asymmetry, can be attributed to a phase lag, e.g., due to the finite propagation time of information concerning the orientation of the magnetic dipole axis. In this case, $\phi_{III}(r')$ is that predicted for the bent disc ($\phi_o'(r')$, say) plus the phase lag $\bar{\phi}'$ due to the propagation time. Assuming that $\phi' \sim r'$, the correction is negligible at small r', but becomes increasingly significant as r' increases. This is illustrated by the difference between symmetric bent plane/hinged plane model and the asymmetric wave model of Eviatar and Ershkovich (1976). The effect of adding $\bar{\phi}'$ to ϕ_o' is to make the curve for S-N crossings flatter and the curve for N-S crossings steeper at large r'. Figure 21 shows that the model of Eviatar and Ershkovich, which includes both bending and a wave propagating outward from the edge of the disc, gives a fit which is qualitatively correct, as noted by Carbary (1980). A better fit is obtained by our model (11) which includes bending and wave propagating outward from r' = 0, as shown in Figure 21. There is no reason to expect that wave generation is strictly limited to the edge of the disc, since the disc is not actually a rigid structure. This result suggests that the waves must actually originate nearer the planet.

Summarizing the results of the axial models, we find that 1) the rotating plane (0-parameter), the bent/hinged plane (1-parameter) and the rotating plane with wave (2-parameter) do not give satisfactory fits to the V1 and V2 current sheet crossings, and they can be eliminated from further consideration; 2) Models which incorporate both bending (i.e., bounded elevation at large distances) and a wave propagating from the edge of the disc give good fits to V2 and fair fits to V1; and 3) the bent rotating disc with a wave propagating from the origin gives good fits to both V2 and V1. The results indicate the need for some bending at a distance $\gtrsim 30\ R_J$, but they do not determine the cause of the bending. The results suggest that the speed with which information concerning the position of the magnetic dipole axis is propagated might be a significant parameter. Table 1 shows that average signal speed is 44 R_J/hr. For the crossings observed between $\sim 25\ R_J$ and $\sim 100\ R_J$, which were used for our fits, this implies a signal propagation time ranging from ~ 0.6 hr to ~ 2.3 hr, which is small

but not negligible compared to Jupiter's rotation period (10 hr).

Non-axial Models. If the shape of the current sheet is influenced by the formation of a tail, then the axial models described above can be a valid approximation only over a small range of longitudes, and they must be inapplicable at large distances. In other words, one is not justified in extrapolating the surfaces described by the axial models very much beyond the regions in which the data for the fits were obtained. In this section we discuss models which might be expected to describe the influence of tail-formation on the current sheet geometry more globally (see the lower part of Figure 19).

i) Rocking Plane. A very simple surface with a tail-like geometry, which gives current sheet crossings of a spacecraft moving behind Jupiter and which retains some information about the orientation of the magnetic dipole axis, is a plane containing the x-axis whose inclination changes by ± 10° with respect to the plane z = 0 in response to the rotation of Jupiter's magnetic dipole axis (see Figure 20). The equation for this surface relative to a fixed frame is

$$z/\tan\alpha = y \sin\phi. \tag{12}$$

The normal to this surface is in the direction $\vec{N} = \sin\phi \tan\alpha\, \hat{Y} + \hat{Z}$, i.e., it is perpendicular to $\hat{X}$ and it rocks back and forth with respect to the z-axis by ± 10°. There are no free parameters.

ii) Rocking Plane/Rotating Disk (RP/RD). The rocking plane model is unrealistic close to the planet where one expects a rotating disc to be a good approximation. A 1-parameter surface which reduces to a rotating disc (4) close to Jupiter and to a rocking plane (12) at large distances is

$$z/\tan\alpha = x \operatorname{sech}(x/a) \cos\phi + y \sin\phi. \tag{13}$$

The surface is described by the vector function $\vec{S} = x\,\hat{X} + y\,\hat{Y} + z(x,y)\,\hat{Z}$ with z given by (13). This can be written in the form

$\vec{r} = \vec{f}(x,\phi) + y\,\vec{g}(\phi)$, where $\vec{f} = x\,\hat{X} + [x \operatorname{sech}(x/a) \cos\phi \tan\alpha]\,\hat{Z}$ and $\vec{g} = \hat{Y} + (\sin\phi \tan\alpha)\,\hat{Z}$, indicating that it is a ruled surface. The base curve is $z = x \operatorname{sech}(x/a) \cos\phi \tan\alpha$ and the rulings are parallel lines which are perpendicular to $\hat{X}$. The rulings intersect the plane $y = 0$ on the base curve and they intersect the plane $z = 0$ on the curve $y = -x \operatorname{sech}(x/a) \cos\phi \tan\alpha$. This surface is illustrated in Figure 20 also.

iii) Bent RP/RD. One can introduce bending in the RP/RD model such that the elevation of the surface is bounded at large distances by the equation

$$z/\tan\alpha = a \operatorname{sech}(x/a) \tanh(x/a) \cos\phi + b \tanh(y/b) \sin\phi. \qquad (14)$$

This contains two parameters, a and b.

iv) RP/RD with Wave. The effects of a wave, or the finite propagation time of information from the disc-region, may be included by adding a phase lag $\bar{\phi} = \Omega\,(x - a)/U$ to ϕ in (13):

$$z/\tan\alpha = x \operatorname{sech}(x/a) \cos[\phi + \Omega\,(x - a)/U] + y \sin[\phi + \Omega\,(x - a)/U]. \qquad (15)$$

v) Shadow. Finally, we add a model in which the current sheeet is 1) a circular disc with radius a close to Jupiter; 2) a surface formed by the boundary of the "shadow" of the disk illuminated by the sun (i.e., consisting of straight lines parallel to $\hat{X}$ and beginning on the boundary of the disc); and 3) the plane $z = 0$ outside the disc and shadow. There is only 1 free parameter, the radius of the disc.

We obtained fits of each of the above non-axial models to the V1 and V2 current sheet crossing times. The results are summarized in Table 2. The simple 0-parameter rocking plane model gives a fair fit to V1 (F1 = 2.3) and a good fit to V2 (F2 = 1.5). The 1-parameter RP/RD model, which reduces to a rotating disc at small x, gives a fair fit to V1 (F1 = 2.3) and a very good fit to V2 (F2 = 1.0). The 1-parameter shadow model gives nearly the same result (F1 = 2.3, F2 = 1.3). Adding bending in the y-direction to the RP/RD model gives a somewhat better fit to V1 (F1 =

1.9), and has no effect on the fit to V2 (F2 = 1.0). Adding a wave to the RP/RD model instead of bending gives a somewhat worse fit to V1 (F1 = 2.5) than the RP/RD model (F1 = 2.3) and only a slightly better fit to V2 (F2 = 0.9) than the RP/RD model (F2 = 1.0).

The validity of the RP/RD model can also be demonstrated by 1) plotting the observed ϕ_D of Jupiter's magnetic dipole axis at the times of the current sheet crossings versus the spacecraft positions at these times, and 2) comparing these ϕ_D with the predictions of the RP/RD model. These results are shown in Figure 22 for the V2 tail current sheet crossings. The model gives an excellent fit to both the S-N and the N-S crossings over the entire range of distances, $24\ R_J \lesssim x \lesssim 72\ R_J$. Figure 22 also shows the observed z-positions of the spacecraft at the times of the crossings as a function of x together with the predictions of the RP/RD model. The model gives a very good fit to z(x), the scatter being only $\sim \pm 1\ R_J$.

Summarizing the results for the non-axial models, we see that the 1-parameter RP/RD model, which reduces to a rocking plane at large x and a rotating disc at small x, provides an accurate description of the V1 and V2 current sheet crossing times. Wave propagation seems to be a relatively unimportant effect in the class of non-axial models. Some bending at large distances in the y-direction is suggested by V1, but it does not improve the fits appreciably. The 1-parameter shadow model is almost as good as the RP/RD model. The essential feature seems to be the extension of the current sheet parallel to the x-axis with a limited elevation along x at distances $\gtrsim 30\ R_J$.

Finally, let us compare the axial models with the non-axial models. The 0-parameter rocking plane model gives much better fits to the data than the 0-parameter rotating plane model, indicating that in the absence of other effects the "tail" geometry (i.e., a current sheet which remains close to the plane z = 0) is more important at large distances downstream ($x \gtrsim 20\ R_J$) than the disc geometry. The disc geometry is important close to Jupiter, however. Allowing a wave in the axial models (Kivelson et al., 1976) still does not give an acceptable fit to the V2 data, and it has little effect on the non-axial models. The results suggest that a limited

elevation at large distances down the tail seems to be the essential feature of the current sheet. This is intrinsic in the non-axial models, and introducing it in the axial models by means of "bending" gives a significantly better fit to the data. The maximum elevation indicated by our results is $\sim a \tan \alpha \lesssim 5\ R_J$; an upper limit on the elevation is $\sim 10\ R_J$. It is interesting to note that none of the models gave us as good a fit for the V1 data as for the V2 data, suggesting that at the position of V1 there are spatial distortions of the current sheet geometry, perhaps transitional, which are not present along the V2 trajectory.

Comparison of Models by Statistical Testing. To obtain a clearer indication of how well the various models investigated fit the measured data in both an absolute sense and also relative to one another, a pair of statistical tests were adapted and applied. They consisted of a χ^2 "goodness-of-fit" test (Meyer, 1975) and an "equality of variances" F-test (Pollard, 1977). Central to both tests for a given model in this application was the rms residual, which is derived from the sum of the squared residuals, $Z_{model}-Z_{obs}$. It is only appropriate to apply the tests if the residuals are normally distributed. Although the samples were small in each case, distributions for combined (N = 40) V1 and V2 residuals were found to be at least approximately Gaussian for the models under study.

In the goodness-of-fit test, models were classified as providing unacceptable fits (should be rejected) if the rms exceeded an upper limit value given by

$$rms_{max} = \frac{\chi^2}{N},$$

where N is the number of data points and χ^2 was determined from a standard χ^2 table for probability 0.05 (that the experimental rms value would be lower than the tabular value strictly by chance) and degrees of freedom given by $df = N - n_p$ with n_p the number of parameters in the mathematical model. According to this scheme, the only model giving a satisfactory fit for V1 was the bent plane with wave-2 axial model. For V2, acceptable fits were given by the hinged plane with wave, bent plane with wave-1 and bent

plane with wave-2 among the axial models, and the RP/RD, bent RP/RD and RP/RD with wave among the nonaxial models, with a borderline result for the shadow model.

Among the acceptable fits, it was of interest to test whether or not there was a statistically significant difference in the goodness-of-fit between them. For this we used a standard table of the upper 5 per cent points of the F-distribution. The test statistic

$$F_{test} = \frac{S_1^2}{\sigma_1^2} \frac{S_2^2}{\sigma_2^2}$$

was derived from the rms's for pairs of models to be compared, letting $\sigma_1^2 = \sigma_2^2$. Only if a variance ratio exceeded the tabular F-value appropriate for $N_1-1 = N_2-1 = 19$ could it be concluded that there was a significant difference in goodness-of-fit between a given pair of models, with the model having lower rms adjudged the superior model.

Summarizing the most important results of this test, we found no significant difference in the quality of fit between the 1-parameter bent RP/RD model (the best all-around nonaxial model) and the 2-parameter bent plane with wave-1 axial model (essentially the Eviatar-Ershkovich model) for either V1 or V2. In comparing the bent RP/RD model and the bent plane with wave-2 model (wave from r = 0), we found no significant difference for V2, but for V1 the axial model was found to provide a better fit to the data. This result was implicit in the χ^2 test results. Thus, in the region where the tail is developing, the nonaxial model introduced here does not appear to address the motions of the current sheet outside the rigid disc region but still not within the tail proper as well as does the best axial model considered. Within the more fully developed tail, as observed by V2, the simpler nonaxial model does as well as the axial model in terms of fitting the observations and is <u>superior</u> in terms of having fewer parameters.

<u>Motion of the Jovian Current Sheet</u>. Both the axial and non-axial

models discussed above assume that the current sheet moves periodically, with a period $2\pi/\Omega$ equal to Jupiter's rotation period. In the non-axial models, the speed in the z-direction is, from (2),

$$V(t) = dz/dt = [-f \sin(\phi + \bar{\phi}) + g \cos(\phi + \bar{\phi})]\, \Omega \tan \alpha.$$

The speed is the maximum, V_m, when $d^2z/dt^2 = -f \cos(\phi_m + \bar{\phi}) - g \sin(\phi_m + \bar{\phi}) = -z/\tan \alpha = 0$, i.e., when the current sheet passes through the equatorial plane. This gives $|V_m| = (\Omega \tan \alpha)|\, g/\cos(\phi_m + \bar{\phi})| = 0$. The phase ϕ_m at maximum V is given by $\tan(\phi_m + \bar{\phi}) = -f/g$. For example, in the rocking plane model, $f = 0$ $g = y$ and $\bar{\phi} = 0$, giving $\phi_m = 0$ and $V_m = (\Omega \tan \alpha)\, y$. Thus for a spacecraft at $y = 40\ R_J$ and $z = 0$, $V_m = \sim 4.5\ R_J/hr$. For a spacecraft at $z \neq 0$, $V = [V_m^2 - (\Omega z)^2]^{1/2}$.

The axial models (3) give $V = dz/dt = (\tan \alpha)(\Omega h) \sin(\phi' - \bar{\phi}')$. In this case $V_m = \Omega h \tan \alpha$ and the maximum speed occurs when $\phi' = \bar{\phi}'$. For the rotating plane, $h = r'$ and $V_m = \Omega r' \tan \alpha$. For a spacecraft at $r' = (x^2 + y^2)^{1/2} = 70\ R_J$, $V_m = 8\ R_J/hr$. The rotating disc with wave model gives the same result for V_m, but the maximum speed occurs at a different phase. The bent disc model gives $V_m = \Omega a \tanh(r'/a) \tan \alpha \leq \Omega a \tan \alpha$ with $a \lesssim 25\ R_J$. For a spacecraft at $r' \gtrsim 25\ R_J$, this model gives $V_m \lesssim 3\ R_J/hr$.

Summarizing, our results suggest that the maximum speed of the current sheet along z is $\lesssim 5\ R_J/hr$, depending on the maximum elevation of the current sheet and on the spacecraft position.

Current Sheet Thickness. With a model for current sheet motion and the observed durations of the diamagnetic depression of field strength by plasma sheet ions, it is possible to estimate the thickness τ of the magnetotail plasma sheet using $\tau = V\Delta t$. One can also attempt to estimate the thickness of the embedded "neutral" sheet using the observed durations of field direction variation, which coincide with the intervals over which the minimum variance analysis was performed. We have derived thicknesses for these regions of the Jovian tail using the RP/RD model and assuming that (1) neglecting terms of order α^2, the direction of motion of the

sheet, and consequently the direction along which the thickness is estimated, is the $\hat{Z}$ direction (perpendicular to the Jovian equatorial plane); (2) the component of spacecraft velocity in the $\hat{Z}$ direction during the analysis period was small ($\sim$ 0.05 R_J/hr on average) and thus negligible relative to the sheet's speed in that direction; and (3) sheet motion during the traversals considered was steady. The last assumption is the one most likely to have been false, at least in some of the cases in which the observed field variations had the irregular character suggestive of unsteady motions.

In Table 3 we have tabulated the results for 10 sheet crossings in which the RP/RD model predicted quite accurately the z coordinate and ϕ_D for the traversal. This is important since the predicted V_Z for the sheet varies with z from a maximum at z = 0 to V_Z = 0 at z_{max}. We have included in the table the y coordinate of the crossing point in each case, since for rigid rotations of the sheet about the tail (x) axis the linear speed of the sheet in its normal direction increases as a function of y. We have given the sheet speeds in both R_J/hr and km/s. The signs are consistent with the crossings being either south-to-north (sheet moving south, therefore $- V_Z$) or north-to-south ($+ V_Z$). It can be seen that the estimated plasma sheet thicknesses τ_{PS} range from 3.6 to 6.5 R_J. The average for the 10 cases was 4.8 ± 0.3 R_J, with the probable error given by $\pm \sigma/ N$. This result is consistent with the current sheet thickness estimate of $\sim$ 4.2 R_J from plasma wave measurements (Barbosa et al., 1979) and with that in the inner magnetosphere sheet model of Connerney et al. (1981); it is somewhat larger than the estimates of $\sim$ 1 R_J by Smith et al. (1974) and 2.2 - 3.4 R_J by Kivelson et al. (1978) based on current sheet observations in other regions of the magnetosphere.

Of the thickness values given in Table 3, the largest (6.5 R_J) corresponds to a traversal during possibly unsteady sheet motion, and therefore the actual thickness was probably less in that case. That applies also to the last case (τ_{PS} = 5.2 R_J), where there were actually three crossings of the "neutral" sheet. On the other hand, the two crossings for which τ_{PS} = 5.3 R_J had all the appearances of very steady traversals. In summary, while in general the thickness values presented

here should strictly speaking be taken as upper limits, there is strong evidence that at least some of the time the tail plasma sheet may have a thickness of $\sim 5\ R_J$, which is still quite thin relative to a tail radius of $\sim 150 - 200\ R_J$ (i.e., τ 3% of R_T).

As seen in the last column of Table 3, the region of the plasma sheet in which substantially all of the magnetic field directional variation takes place was found to be quite thin indeed, the estimates ranging from 0.08 to 0.62 R_J, with an average of $0.31 \pm 0.06\ R_J$. Thus it constituted on average only $\sim$ 6% of the thickness of the region of diamagnetic field magnitude depression.

SUMMARY AND CONCLUSIONS

In this paper we have presented a number of new results obtained from magnetic field measurements by V1 and V2 in the magnetic tail of Jupiter. These results provide additional evidence for the development of a Jovian magnetotail in response to the interaction between the solar wind and the magnetosphere of Jupiter. In some respects Jupiter's magnetotail resembles that of Earth and in other respects it appears to have unique characteristics. In this section we summarize and briefly discuss the new results that we have presented in terms of both the similarities and differences between the two magnetotail systems.

The decrease in average magnetic field strength in the tail lobes with radial distance from Jupiter has been found by the Voyager spacecraft to follow approximately a simple power law on the large scale, although systematic deviations were observed during portions of the transits. Such deviations may have been predominantly temporal, but they have not as yet been identified as such through correlation with specific major changes in the solar wind as observed by the supporting Voyager in each case. Therefore spatial variations in field magnitude due to possible structural differences in different tail regions cannot be ruled out. The rate of decrease of $r^{-1.36}$ from V2, probably significantly different from that observed by P10 outbound ($r^{-1.70}$), suggests a less rapid decrease in field

magnitude with distance in the tailward direction than in the dawn and predawn magnetosphere. The observed lobe field magnitude r-dependence represents, however, a more rapid rate of decrease (for r in units of planetary radii) than was found for the earth's magnetotail, where the power law exponent was found to lie between -0.3 and -0.7. This suggests either a relatively greater degree of flaring of the tail field at Jupiter, a higher rate of closure of the field across the current sheet, at least in the near-planet region of the tail, or both.

From an investigation of the radial distance dependence of the azimuthal and radial field components we conclude that the radial variation in $B_\phi/\rho B_\rho$ observed by V1 and V2 inside 40 R_J is not unambiguously consistent with the uniform radial out-flow model derived from P10 measurements; outside 40 R_J it does not provide a conclusive test, because there the tail field configuration produces a slowly-varying average value of $B\phi/\rho B_\rho$ that approximately mimics the result expected for the spiral field configuration of the model.

The tail current sheet at Jupiter consists of a plasma sheet and embedded "neutral" sheet, qualitatively similar in appearance to the sheets in the geomagnetic tail. In Jupiter's case, however, the tail sheet is an extension of a current "disc" which surrounds the planet. Beyond 20 R_J, the sheet is populated by hot protons and heavier nuclei (e.g., oxygen) of energies from 10 - 30 keV (Barbosa et al., 1979; Lanzerotti et al., 1980). We found an average thickness of 4.8 R_J for 10 sheet traversals. Using the average field strengths observed during these crossings gives a sheet thickness range of 6 - 50 gyroradii (R_L) for 30 keV O^+ ions and greater by a factor of 4 for protons of the same energy. This may be compared to the thickness range in proton gyroradii of 6 - 36 R_L for magnetic hole current sheets in the solar wind (Fitzenreiter and Burlaga, 1978). Considering that R_L for 30 keV protons is greater than that for solar wind protons by a factor of $\sim$ 60, it can be seen that the Jovian tail sheet is several hundred times broader than typical solar wind sheets. Still, it is relatively thin in comparison with the scale of the magnetotail. This is in contrast with the terrestrial plasma sheet, which can be 40% of the radius of the tail in thickness.

As a result of both the limited body of single-spacecraft data from each flyby and the fact that the current sheet is almost always in motion, including both oscillatory motions and superimposed irregular fluctuations, it has not been possible to identify expansions and contractions of plasma sheet thickness, although such variations probably occur. Also, there is too little data to demonstrate conclusively such structural details as the east-west curvature shown by Fairfield (1980) to be a major feature in the shape of the earth's tail current sheet.

We find that the RP/RD model, a relatively simple, one-parameter model of the sheet surface which reduces to a rocking plane at large distances and to a rotating disc at small distances, provides a satisfactory description of the observed sheet in the Jovian tail, within the constraints of a rather restricted data set. The distributions of sheet normals derived from minimum variance analysis of the internal structure of the sheets support the view that the distant tail current sheet is an oscillating plane whose raxis is the Jupiter-sun line. In contrast to the conclusion of Barbosa _et al_. (1979) that the current sheet is distorted toward the rotational equator beyond 80 R_J, we find that the tail sheet bends toward the rotational equator perhaps as near as $\sim$ 25-30 R_J from Jupiter.

ACKNOWLEDGMENTS

We thank R. F. Thompson, R. J. Fitzenreiter, L. J. Moriarty, and P. Harrison for their programming and data processing assistance, and R. P. Lepping and F. M. Neubauer for their advice in various aspects of this work.

REFERENCES

Barbosa, D. D., D. A. Gurnett, W. S. Kurth, and F. L. Scarf, Structure and properties of Jupiter's magnetoplasma disc, Geophys. Res. Lett., 6, 785, 1979.

Behannon, K. W., Mapping of the earth's bow shock and magnetic tail by Explorer 33, J. Geophys. Res., 73, 907, 1968.

Behannon, K. W., Observations of the interplanetary magnetic field between 0.46 and 1 A. U. by the Mariner 10 spacecraft, Ph. D. Thesis, Catholic University of America; NASA/GSFC X-692-76-2, January 1976.

Behannon, K. W., M. H. Acuna, L. F. Burlaga, R. P. Lepping, N. F. Ness, and F. M. Neubauer, Magnetic field experiment for Voyagers 1 and 2, Space Sci. Rev., 21, 235, 1977.

Bridge, H. S., J. W. Belcher, A. J. Lazarus, J. D. Sullivan, F. Bagenal, R. L. McNutt, Jr., K. W. Ogilvie, J. D. Scudder, E. C. Sittler, V. M. Vasyliunas, and C. K. Goertz, Plasma observations near Jupiter: Initial results from Voyager 2, Science, 206, 972, 1979.

Carbary, J. F., Periodicities in the Jovian magnetosphere: Magnetodisc models after Voyager, Geophys. Res. Lett., 7, 29, 1980.

Connerney, J. E. P., M. H. Acuna, and N. F. Ness, Modeling the Jovian current sheet and inner magnetosphere, J. Geophys. Res., this issue, 1981.

Eviatar, A., and A. I. Ershkovich, Plasma density in the outer Jovian magnetosphere, J. Geophys. Res., 81, 4027, 1976.

Fairfield, D. H., A statistical determination of the shape and position of the geomagnetic neutral sheet, J. Geophys. Res., 85, 775. 1980.

Fitzenreiter, R. J. and L. F. Burlaga, Structure of current sheets in magnetic holes at 1 AU, J. Geophys. Res., 83, 5579, 1978.

Goertz, C. K., Jupiter's magnetosphere: Particles and fields, Jupiter, edited by T. Gehrels, University of Arizona Press, Tucson, Arizona, p. 32, 1976a.

Goertz, C. K., The current sheet in Jupiter's magnetosphere, J. Geophys. Res., 81, 3368, 1976b.

Goertz, C. K., The Jovian magnetodisk, Space Sci. Rev., 23, 319, 1979.

Goertz, C. K., D. E. Jones, B. A. Randall, E. J. Smith, and M. F. Thomsen, Evidence for open field lines in Jupiter's magnetosphere, J. Geophys.

Res., 81, 3393, 1976.

Gurnett, D. A., W. S. Kurth, and F. L. Scarf, The structure of the Jovian magnetotail from plasma wave observations, Geophys. Res. Lett., 7, 53, 1980.

Hill, T. W., A. J. Dessler, F. C. Michel, Configuration of the Jovian magnetosphere, Geophys. Res. Lett., 1, 1, 1974.

Kivelson, M. G., Jupiter's distant environment, in Physics of Solar Planetary Environments, edited by D. J. Williams, p. 836, Am. Geophys. Union, Wash., D. C., 1976.

Kivelson, M. G., P. J. Coleman, Jr., L. Froidvaux, and R. L. Rosenberg, A time dependent model of the Jovian current sheet, J. Geophys. Res., 83, 4823, 1978.

Lanzerotti, L. J., C. G. Maclennan, S. M. Krimigis, T. P. Armstrong, K. W. Behannon, and N. F. Ness, Statics of the nightside Jovian plasma sheet, submitted to Geophys. Res. Lett., 1980.

Lepping, R. P., and K. W. Behannon, Magnetic field directional discontinuities: 1. Minimum variance errors, J. Geophys. Res., to appear, 1980.

Lepping, R. P., L. F. Burlaga, and L. W. Klein, Jupiter's magnetopause, bow shock, and 10-hour modulated magnetosheath: Voyagers 1 and 2, submitted to Geophys. Res. Lett., 1980.

Lepping, R, P., L. F. Burlaga, L. W. Klein, J. M. Jessen, and C. C. Goodrich, Observations of the magnetic field and plasma flow in Jupiter's magnetosheath, J. Geophys. Res., this issue, 1981.

Meyer, S. L., Data Analysis for Scientists and Engineers, John Wiley and Sons, New York, 1975.

Mihalov, J. D., D. S. Colburn, R. G. Currie, and C. P. Sonett, Configuration and reconnection of the geomagnetic tail, J. Geophys. Res., 73, 943, 1968.

Ness, N. F., M. H. Acuna, R. P. Lepping, L. F. Burlaga, K. W. Behannon, and F. M. Neubauer, Magnetic field studies at Jupiter by Voyager 1: Preliminary results, Science, 204, 982, 1979a.

Ness, N. F., M. H. Acuna, R. P. Lepping, K. W. Behannon, L. F. Burlaga, and F. M. Neubauer, Jupiter's magnetic tail, Nature, 280, 799, 1979b.

Ness, N. F., M. H. Acuna, R. P. Lepping, L. F. Burlaga, K. W. Behannon, and F. M. Neubauer, Magnetic field studies at Jupiter by Voyager 2:

Preliminary results, Science, 206, 966, 1979c.

Northrop, T. G., C. K. Goertz, and J. F. Thomsen, The magnetosphere of Jupiter as observed by Pioneer 10, 2, non-rigid rotation of the magnetodisc, J. Geophys. Res., 79, 3579, 1974.

Parker, E. N., Dynamical properties of the magnetosphere, in Physics of the Magnetosphere, edited by R. L. Carovillano, J. F. McClay, and H. R. Radoski, p. 3, D. Reidel Pub. Co., Dordrecht, Holland, 1967a.

Parker, E. N., Small-scale nonequilibrium of the magnetopause and its consequences, J. Geophys. Res., 72, 4365, 1967b.

Pollard, J. H., A Handbook on Numerical and Statistical Techniques, Cambridge University Press, Cambridge, England, 1977.

Schulz, M., Jupiter's radiation belts, Space Sci. Rev., 23, 277, 1979.

Smith, E. J., L. Davis, Jr., D. E. Jones, P. J. Coleman, Jr., D. S. Colburn, P. Dyal, C. P. Sonett, and A. M. A. Frandsen, The planetary magnetic field and magnetosphere of Jupiter: Pioneer 10, J. Geophys. Res., 79, 3501, 1974.

Smith, E. J., L. Davis, D. E. Jones, P. J. Coleman, Jr., D. S. Colburn, P. Dyal, and C. P. Sonett, Jupiter's magnetic field, magnetosphere, and interaction with the solar wind: Pioneer 11, Science, 188, 451, 1975.

Smith, E. J., L. Davis, Jr., and D. E. Jones, Jupiter's magnetic field and magnetosphere, Jupiter, edited by T. Gehrels, p. 788, University of Arizona Press, Tucson, Arizona, 1976.

Sonnerup, B. U. Ö., Magnetopause structure, ISEE Workshop, Space Sciences Laboratory, University of California, Berkeley, December 10, 1977.

Sonnerup, B. U. Ö, Magnetopause and boundary layer, in Physics of Solar Planetary Environments, edited by D. J. Williams, p. 541, Am. Geophys. Union, Wash., D. C., 1976.

Sonnerup, B. U. Ö., and L. J. Cahill, Magnetopause structure and attitude from Explorer 12 observations, J. Geophys. Res., 72, 171, 1967.

Van Allen, J. A., D. N. Baker, B. A. Randall,, M. F. Thomsen, D. D. Sentman, and H. R. Flindt, Energetic electrons in the magnetosphere of Jupiter, Science, 183, 309, 1974.

TABLE 1

Axial Models

Description	Equation	Fit RMS F1	Fit RMS F2	Disc Size (R_J) a_1	Disc Size (R_J) a_2	Wave Speed (R_J/hr) U_1	Wave Speed (R_J/hr) U_2
Rotating Plane	(5)	5.0	4.9	-	-	-	-
Hinged Plane	(6)	3.5	2.1	28	23	-	-
Bent Plane	(7)	3.5	2.1	30	24	-	-
Rotating Plane w. Wave	(8)	2.0	3.4	6	22	46	43
Hinged Plane w. Wave	(9)	2.2	1.2	33	29	30	41
Bent Plane w. Wave-1	(10)	2.1	1.2	37	32	27	37
Bent Plane w. Wave-2	(11)	1.2	0.9	64	39	53	71

TABLE 2

Non-Axial Models

Description	Equation	Fit RMS F1	Fit RMS F2	Scale Length (R_J) a_1	Scale Length (R_J) a_2	Wave Speed(R_J/hr) U_1	Wave Speed(R_J/hr) U_2
Rocking Plane	(12)	2.3	1.5	-	-	-	-
Rocking Plane/Rotating Disc (RP/RD)	(13)	2.3	1.0	10	24	-	-
Bent RP/RD	(14)	1.9	1.0	10,64	32,94*	-	-
RP/RD w. Wave	(15)	2.5	0.9	7	20	200	170
Shadow	See text	2.3	1.3	34	32	-	-

*When scale lengths are given in pairs (a,b), a is along x direction, b along y direction.

TABLE 3

Estimated Current Sheet Velocity and Thickness*

	DAY/TIME	$r(R_J)$	$y(R_J)$	$V_Z(R_J/hr)$	$V_Z(km/sec)$	$T_{PS}(R_J)$	T_{NS} $(R_J;$	$10^4 km)$
1.	192/0530	24.2	2.4	-1.6	-32.5	4.9	0.08	.58
2.	192/1015	27.0	4.7	1.8	34.9	5.3	0.62	4.42
3.	192/1520	29.9	7.0	-1.8	-36.4	5.3	0.21	1.50
4.	193/0120	35.6	11.6	-2.0	-39.4	3.6	0.38	2.71
5.	193/1125	41.2	16.2	-2.2	-43.1	3.6	0.15	1.07
6.	194/1400	55.4	27.6	2.9	58.1	4.8	0.49	3.50
7.	195/0323	62.4	33.2	-3.0	-60.0	4.5	0.45	3.20
8.	195/1320	67.4	37.2	-3.2	-64.2	6.5	0.18	1.28
9.	195/2320	72.4	41.2	-3.6	-70.7	4.3	0.18	1.28
10.	196/0620	76.0	43.9	3.9	77.2	5.2	0.39	2.78

(*Based on RP/RD model and assuming steady motion)

FIGURE CAPTIONS

FIGURE 1 Voyager 1, Voyager 2, and Pioneer 10 Jupiter encounter trajectories in planetocentric orbital coordinates (x-y plane is the orbital plane, + x toward the sun, and + z northward). The day of the year is labeled on the trajectories. Model magnetopause and bow shock curves shown are described by Lepping *et al.* (1980).

FIGURE 2 Magnetic fields measured between planetocentric distances of 13 and 139 R_J by Voyager 1 outbound at Jupiter. Given are the 16-minute average magnetic field magnitude B in nanoteslas (nT), field direction in heliographic longitude λ and latitude δ, and rms deviation in nT. λ is measured in a plane parallel to the sun's equator with $\lambda = 180°$ in the sunward direction. $\delta = 90°$ in northward with respect to that plane. Note the absence of complete current sheet traversals beyond 80 R_J as given by the field azimuth λ (see text).

FIGURE 3 Continuation beyond $r \approx 139\ R_J$ of Voyager 1 outbound observations. Magnetopause crossings are indicated by vertical dashed lines. As can be seen, there may have been additional crossings of the tail current sheet before the MP was reached.

FIGURE 4 Magnetic fields measured between planetocentric distances of 10 and 108 R_J by Voyager 2 outbound at Jupiter in same format as Figure 2. Note that in this case the frequency of current sheet traversals changed beyond $r \approx 85\ R_J$.

FIGURE 5 Continuation of Voyager 2 outbound observations between 108 and 194 R_J. In this case, complete traversals cease beyond $r \approx 135\ R_J$ but then may reoccur near the boundary, which is delineated by 7 traversals.

FIGURE 6 Continuation of Voyager 2 outbound observations from 194 to

276 R_J. Note extended period during which the spacecraft was back inside the magnetosphere.

FIGURE 7 Projection of hourly average magnetic field components on the solar magnetospheric (SM) x-y plane along the Voyager 1 and 2 outbound trajectories. Only the field vectors corresponding to alternate hours have been plotted for clarity. The data show that the field is distorted from magnetic meridian planes near the dawn terminator and bent back to parallel the magnetopause (MP) boundary. The MP shown is the Voyager 2 model boundary.

FIGURE 8 Voyager 2 hourly average SM x-z (above) and y-z (below) magnetic field components. All hours have been plotted for more complete coverage in these views. Note in the upper panel the predominance of north lobe (outward-directed) fields as a result of the increasingly northerly location of the Voyager 2 outbound trajectory relative to the mean current sheet position. Also note in both panels the marked contrast between magnetosheath and tail field orientation, although during the outermost period in the tail more variation in the direction of the field was observed than in the near tail.

FIGURE 9 Variation of average magnetotail lobe field with Jovicentric distance for both Voyagers 1 and 2 and Pioneer 10. In addition to the observed variations with increasing r the least squares best fit inverse power law decreases are shown as solid curves. The best fit power law exponents are also given for each data set.

FIGURE 10 Relationship between the radius of the Jovian magnetic tail and field strength, assuming conservation of polar cap magnetic flux in the magnetic tail. θ_{PC} is the angular half-width of the polar cap region.

FIGURE 11 Variation of Voyager 1 hourly average $B_\phi/\rho B_\rho$ with Jovicentric distance, where B_ϕ and B_ρ are the azimuthal and radial components of the magnetic field, respectively, in System III coordinates, and $\rho \equiv r$ is the radial distance. The observed variations are compared with two inverse power law variations.

FIGURE 12 Variation of Voyager 2 hourly average $B_\phi/\rho B_\rho$ with Jovicentric distance, similar to the Voyager 1 variation shown in Figure 6. Note that in both cases there is a change by a factor of ~ 10 between $\rho = 20$ and $\rho = 80\ R_J$ in contrast with the Pioneer 10 variation of at most by a factor of 4 (Goertz et al., 1976).

FIGURE 13 Average magnitude, B, and direction, λ (longitude) and δ (latitude) of the magnetic field in heliographic coordinates (see Figure 2 for definition) during a traversal of the current sheet by Voyager 1 at a radial distance of $\sim 34\ R_J$. Also given is the rms deviation of the total field over the 9.6s averaging period.

FIGURE 14 Magnetic field measurements during a crossing of the distant tail current sheet ($r = 92\ R_J$) by Voyager 2. The format of the data is the same as for Figure 10. Note the greater variability of the field than was seen in the previous figure. This is particularly characteristic of crossings in the deep tail ($r > 80\ R_J$). The five minute interval indicated refers to Figure 12.

FIGURE 15 High resolution (60ms) magnetic field Cartesian components (heliographic coordinates) and total field magnitude during the current sheet traversal shown in Figure 11. Although fluctuations were seen throughout the crossing of the sheet, no coherent waves were detected.

FIGURE 16 Magnetic field data in heliographic coordinates and minimum

variance hodograms for three Voyager 2 crossings of the tail current sheet. Cases shown illustrate three of the four general classes of field variations found in this analysis of internal sheet structure (see text).

FIGURE 17 Distribution of relative normal component magnitudes for 52 sheet crossings by Voyager 2, where B_z is the magnitude of the component of $\underset{\sim}{B}$ normal to the minimum variance plane (assumed to be the plane of the sheet) and $\langle B \rangle = \langle |\underset{\sim}{B}| \rangle$ is the average total field within the sheet. This distribution does not have the bimodal character found for interplanetary directional discontinuities.

FIGURE 18 Distributions of normal component direction given by latitude, δ_N, (above) and longitude, λ_N, (below) in heliographic coordinates. Note the strong tendency for sheet normals to be directed toward $\delta_N = \pm 90°$, with λ_N predominantly within ±10° of 90° or 270°, where $\lambda_N = 90°/270°$ represents the plane perpendicular to the Jupiter-Sun line.

FIGURE 19 This illustrates the geometry for the axial and non-axial models of the current sheet, and it defines the coordinates and the angles that are used in the text.

FIGURE 20 Illustration of three current sheet models. Top: The rocking plane model, which is believed to be a good approximation at large x. Bottom: The rotating plane (or rotating disc) model, which should be a good approximation only close to Jupiter. Middle: The rocking plane/rotating disc (RP/RD) model which incorporates features of both of the above models, reducing to a rocking plane at large x and to a rotating plane at small x.

FIGURE 21 System III longitude of Voyager 2 at the times of current sheet crossings as a function of radial distance from Jupiter, together with the predictions of three models. The

bent plane and the hinged-disc models predict a symmetry between the S-N and N-S crossings which is not observed. The model of Eviatar and Ershkovich includes in addition a time delay which increases with distance due to a wave propagating from the edge of the disc; this implies the addition of a radial-dependent $\Delta\phi_{III}$ to the prediction for the BP/HP models, which gives a better fit. Allowing the wave to propagate from Jupiter increases $\Delta\phi_{III}$ and gives the best fit to the data.

FIGURE 22 Current sheet elevation (z) and azimuth of the dipole axis, ϕ_D, at the times of current sheet crossings are shown as a function of distance from Jupiter along $\hat{X}$, together with the predictions for these parameters based on a best fit to the rocking plane/rotating disc (RP/RD) model. This one-parameter model gives a good fit to the data over the range of distances that was considered.

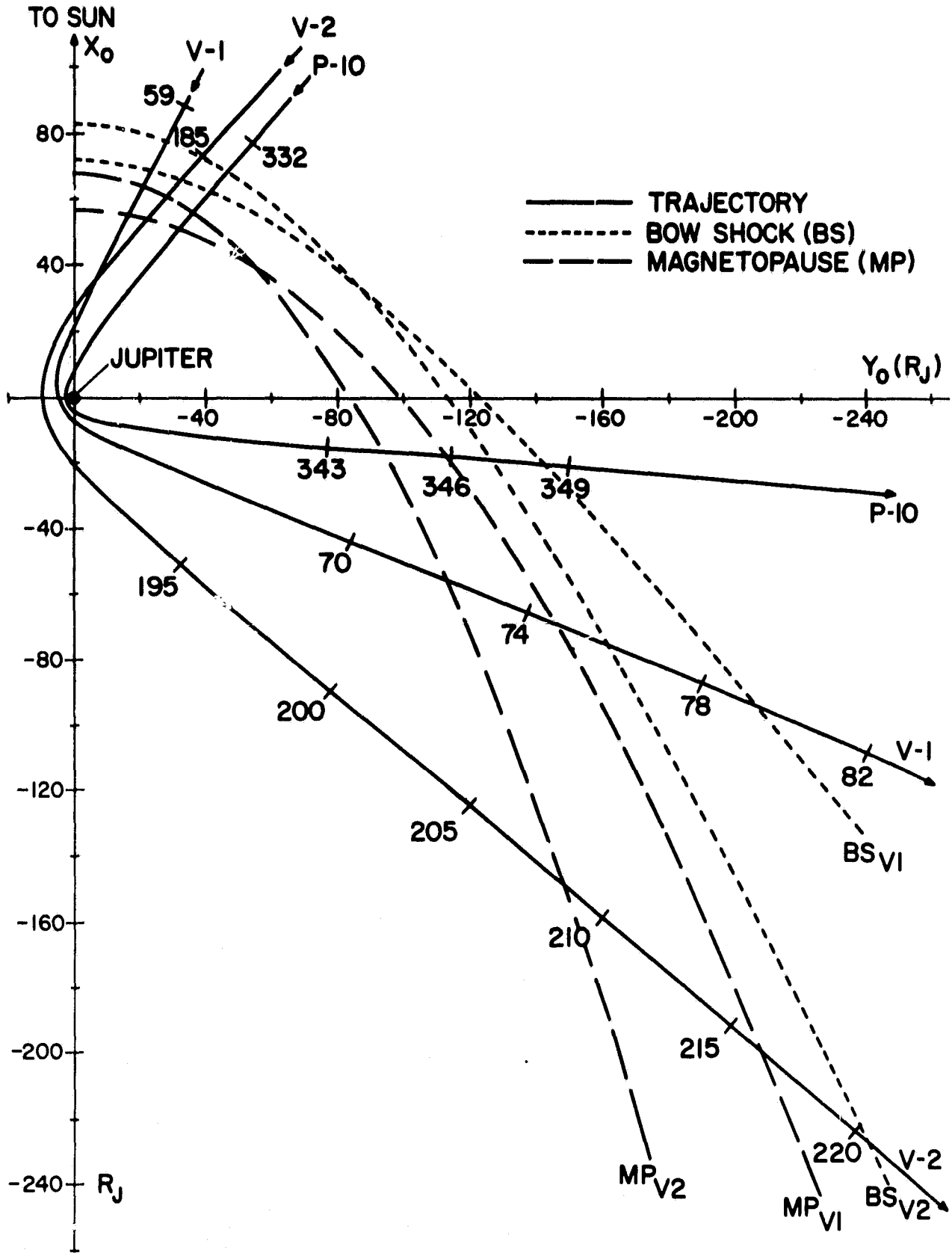
TO SUN
X_0
V-1
V-2
P-10
59
185
332
80
40
TRAJECTORY
BOW SHOCK (BS)
MAGNETOPAUSE (MP)
JUPITER
$Y_0 (R_J)$
-40
-80
-120
-160
-200
-240
343
346
349
P-10
-40
70
195
74
-80
200
78
V-1
82
-120
205
BS_{V1}
-160
210
-200
215
220
V-2
-240
R_J
MP_{V2}
MP_{V1}
BS_{V2}

Figure 1

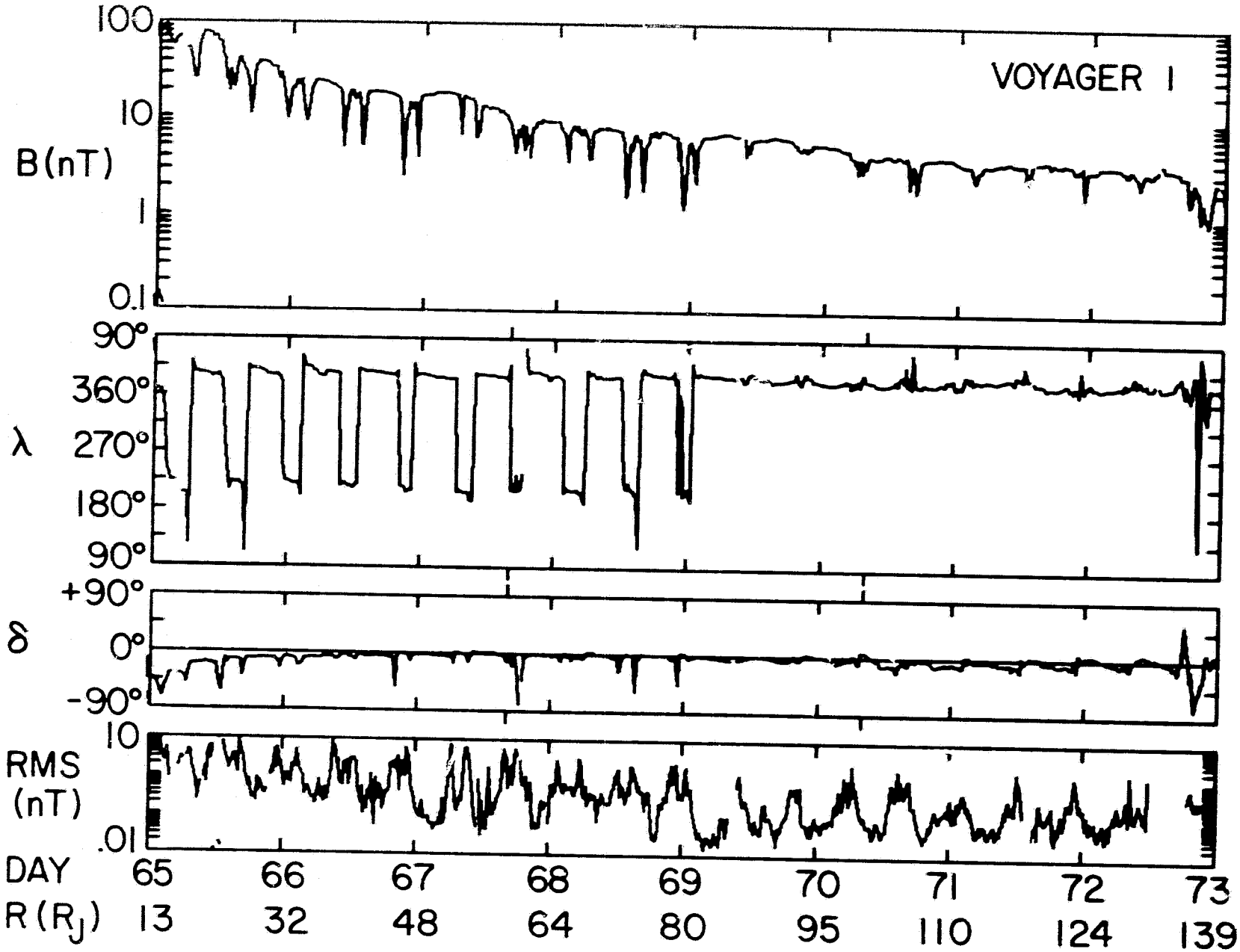
VOYAGER I
B(nT)
100
10
1
0.1
λ
90°
360°
270°
180°
90°
δ
+90°
0°
-90°
RMS
(nT)
10
.01
DAY
65
66
67
68
69
70
71
72
73
R(R_J)
13
32
48
64
80
95
110
124
139

Figure 2

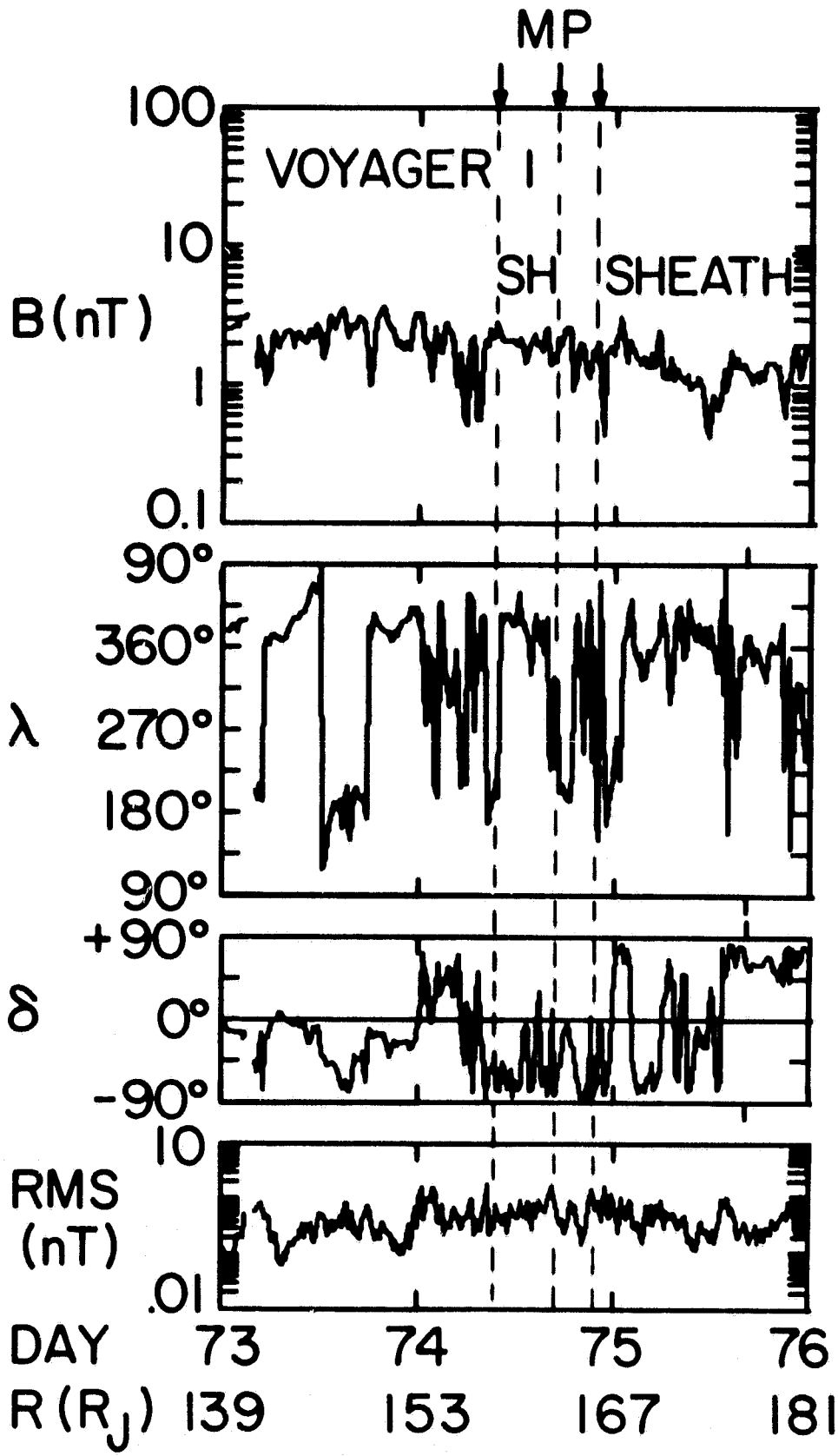
MP
VOYAGER 1
SH
SHEATH
100
10
1
0.1
B(nT)
90°
360°
270°
180°
90°
λ
+90°
0°
-90°
δ
10
.01
RMS
(nT)
DAY
73
74
75
76
R(R_J)
139
153
167
181

Figure 3

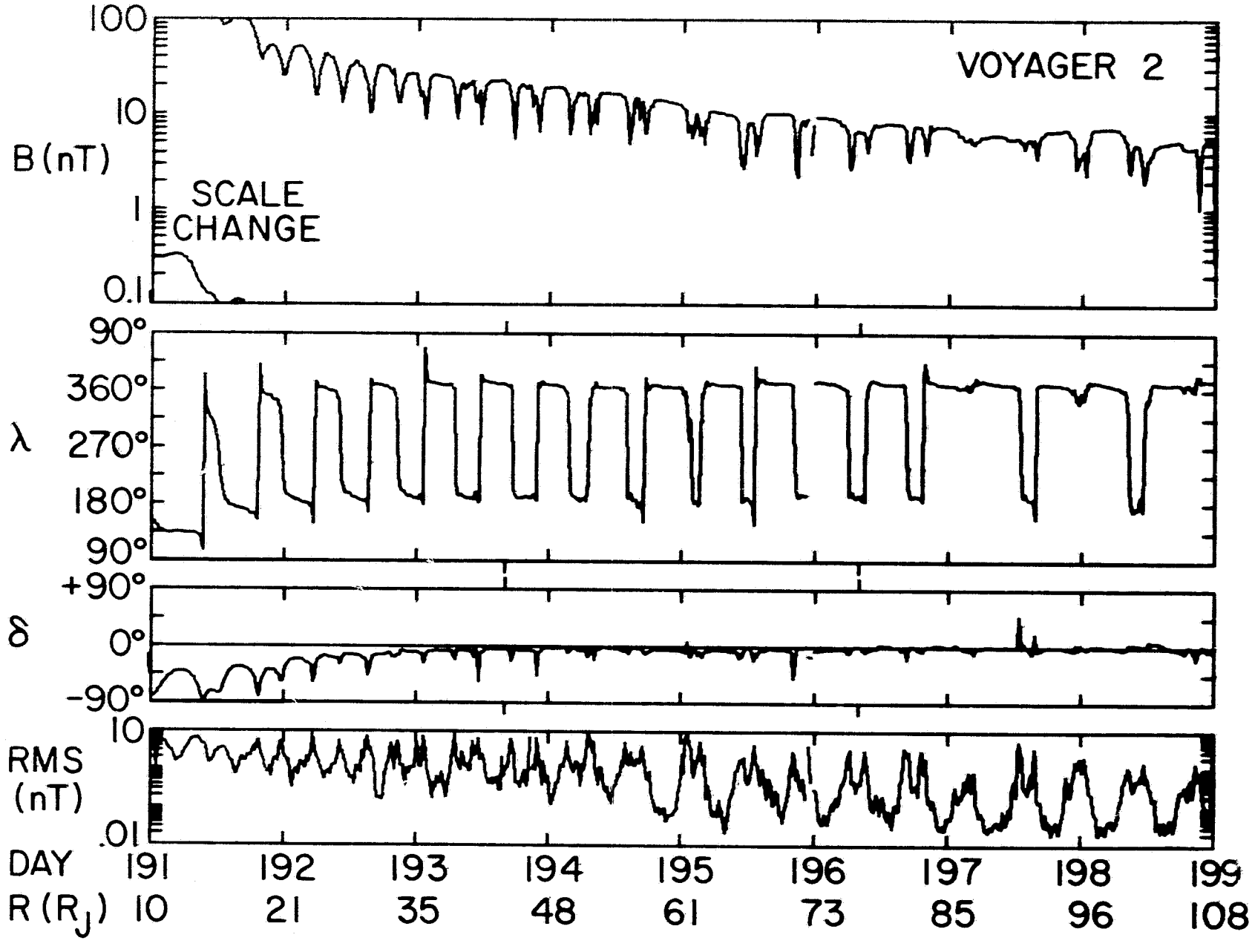
VOYAGER 2
B (nT)
100
10
1
0.1
SCALE
CHANGE
λ
90°
360°
270°
180°
90°
δ
+90°
0°
-90°
RMS
(nT)
10
.01
DAY
191
192
193
194
195
196
197
198
199
R (R_J)
10
21
35
48
61
73
85
96
108

Figure 4

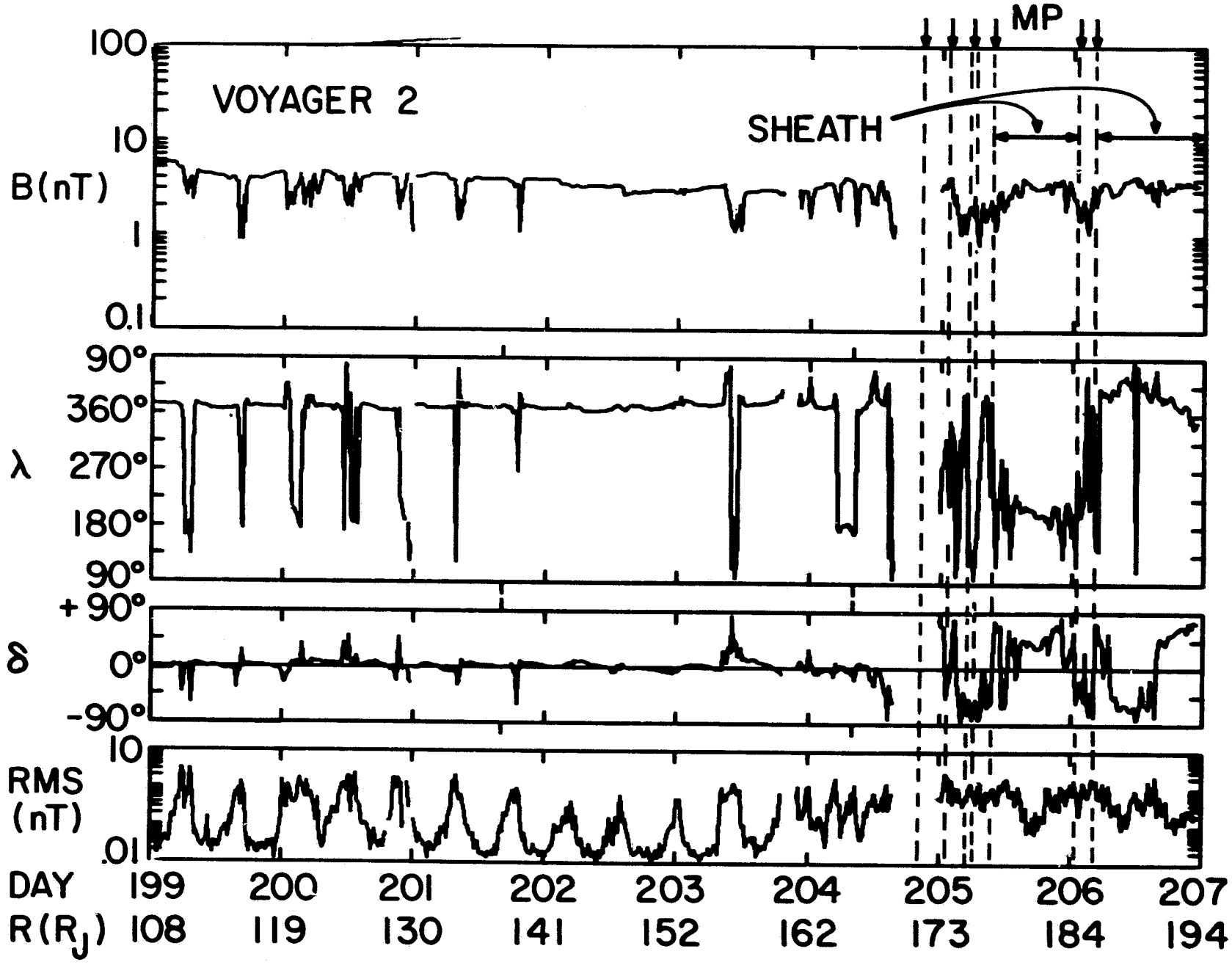
MP
VOYAGER 2
SHEATH
100
10
B(nT)
1
0.1
90°
360°
λ
270°
180°
90°
+90°
δ
0°
-90°
10
RMS
(nT)
.01
DAY 199 200 201 202 203 204 205 206 207
R(R_J) 108 119 130 141 152 162 173 184 194

Figure 5

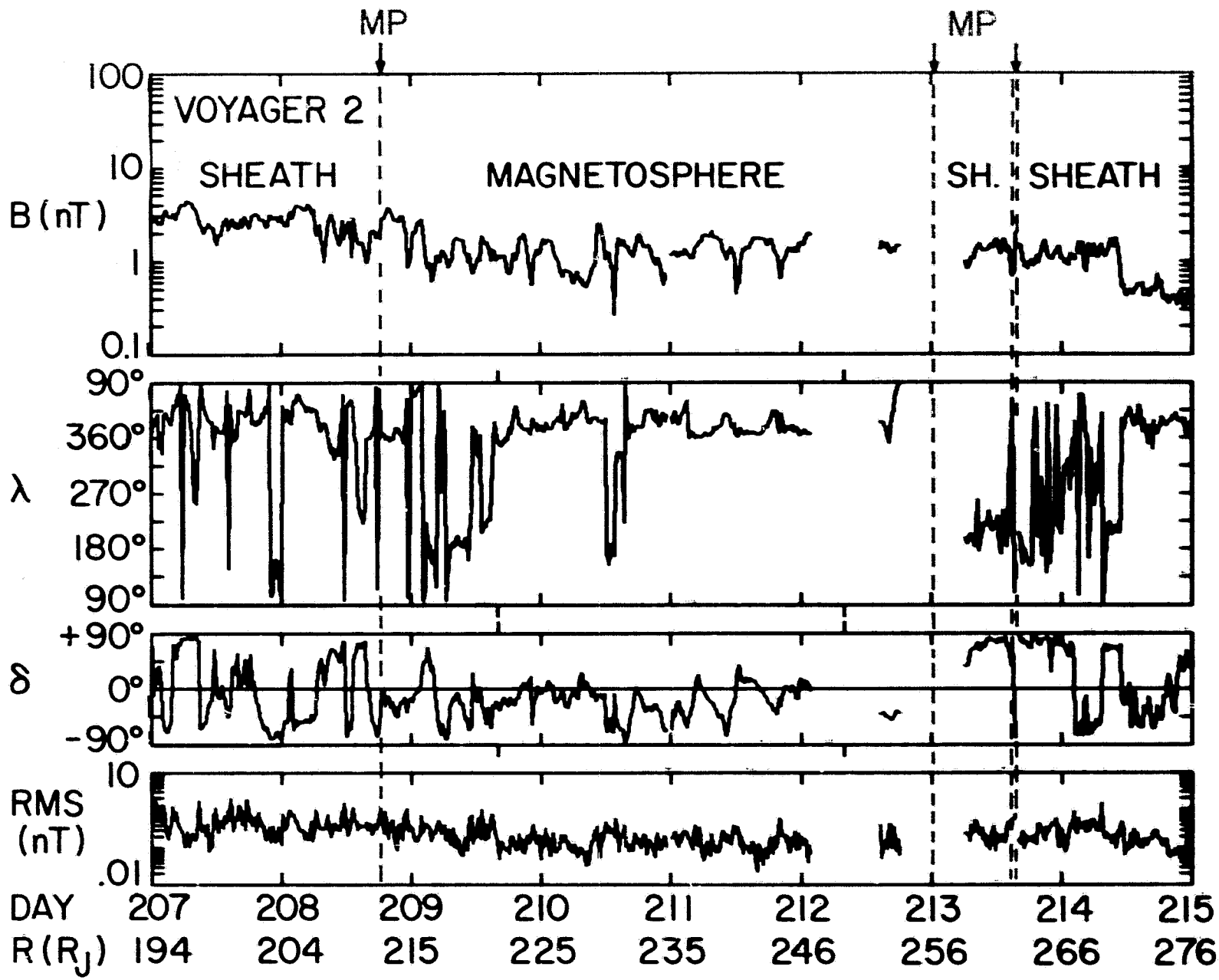
MP
MP
VOYAGER 2
SHEATH
MAGNETOSPHERE
SH.
SHEATH
B (nT)
100
10
1
0.1
λ
90°
360°
270°
180°
90°
δ
+90°
0°
-90°
RMS (nT)
10
.01
DAY
207
208
209
210
211
212
213
214
215
R (R_J)
194
204
215
225
235
246
256
266
276

Figure 6

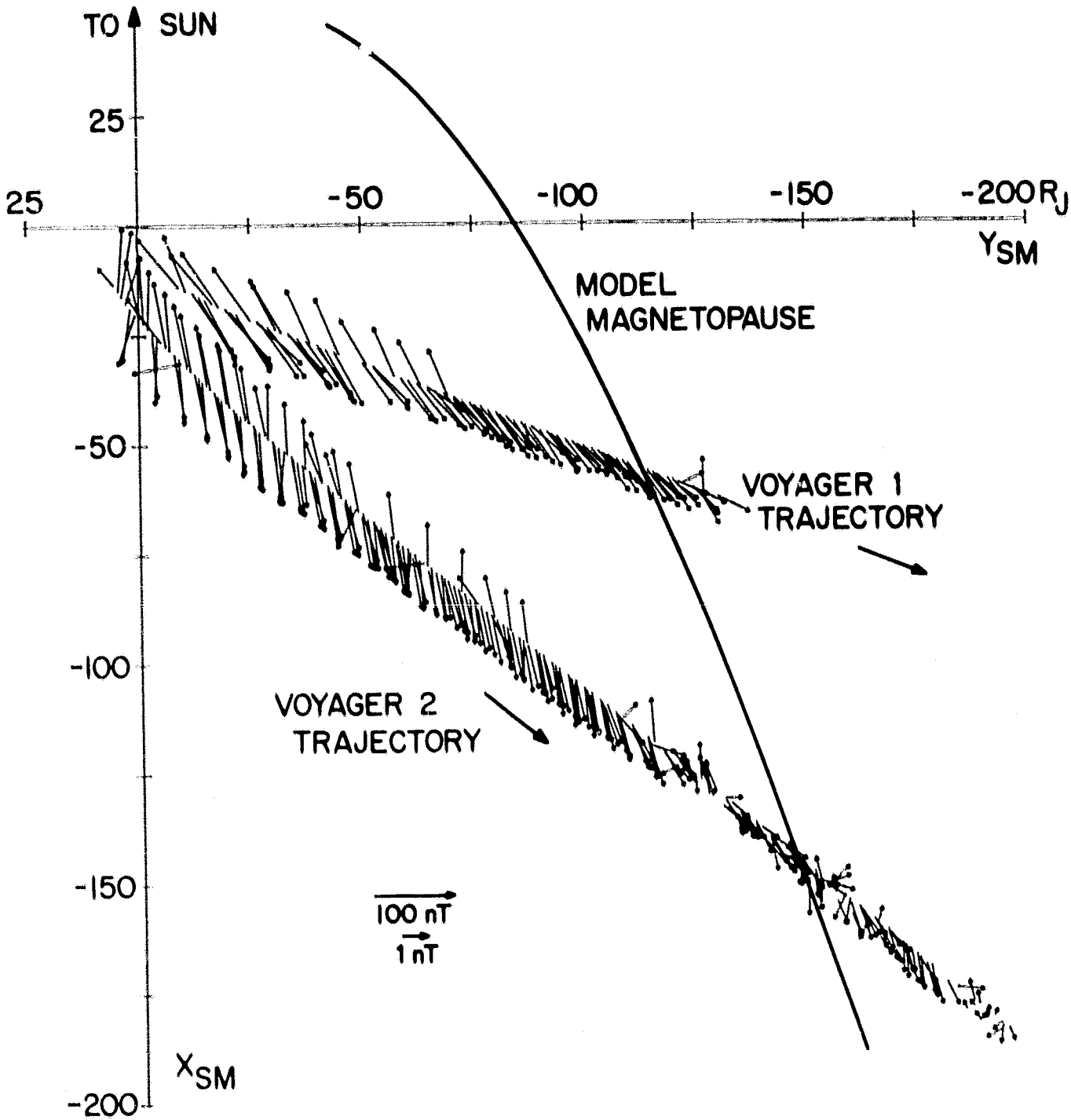
TO SUN
25
25
-50
-100
-150
-200 R_J
Y_{SM}
MODEL
MAGNETOPAUSE
-50
VOYAGER 1
TRAJECTORY
-100
VOYAGER 2
TRAJECTORY
-150
100 nT
1 nT
X_{SM}
-200

Figure 7

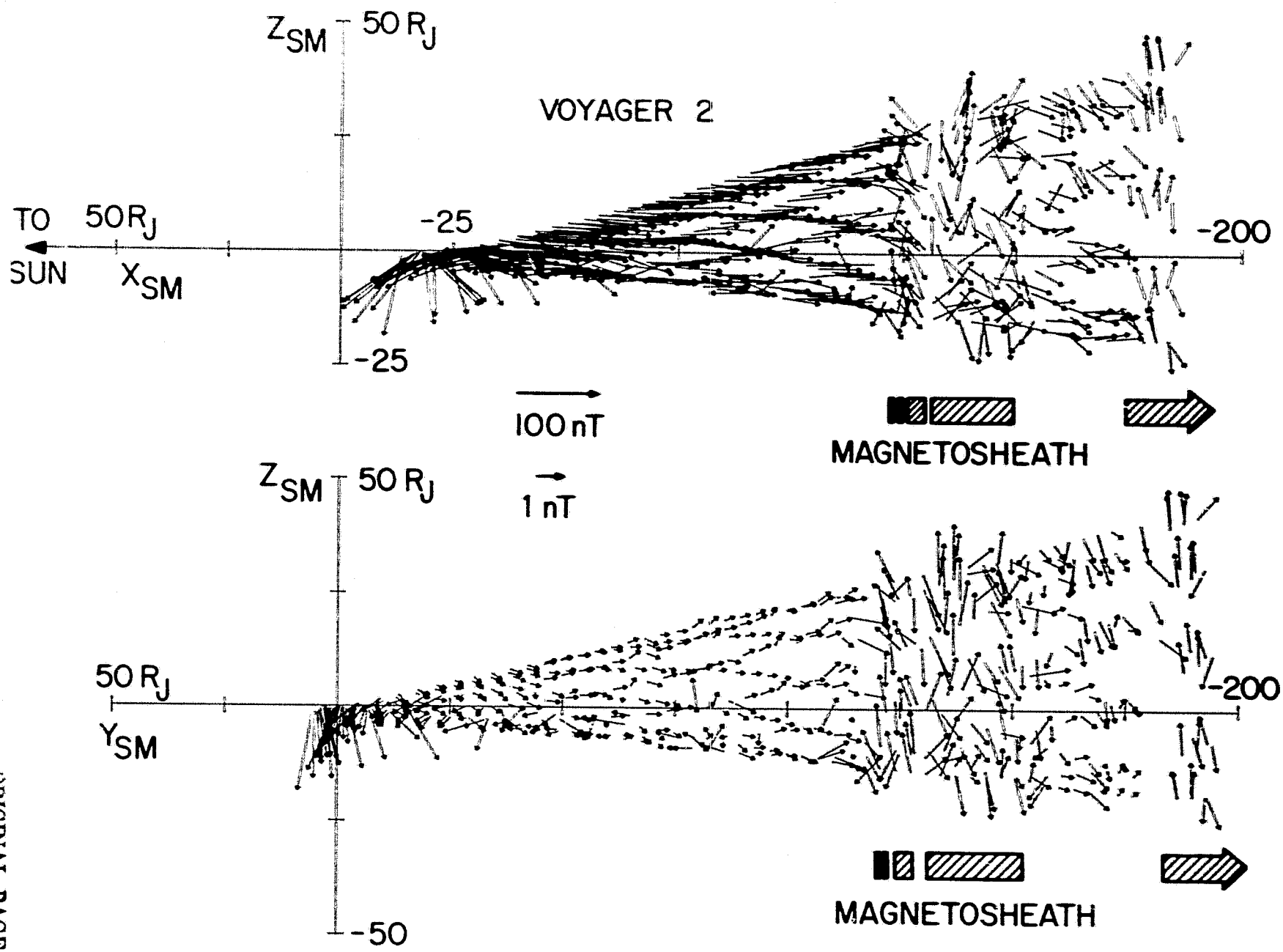

Figure 8

ORIGINAL PAGE IS
OF POOR QUALITY

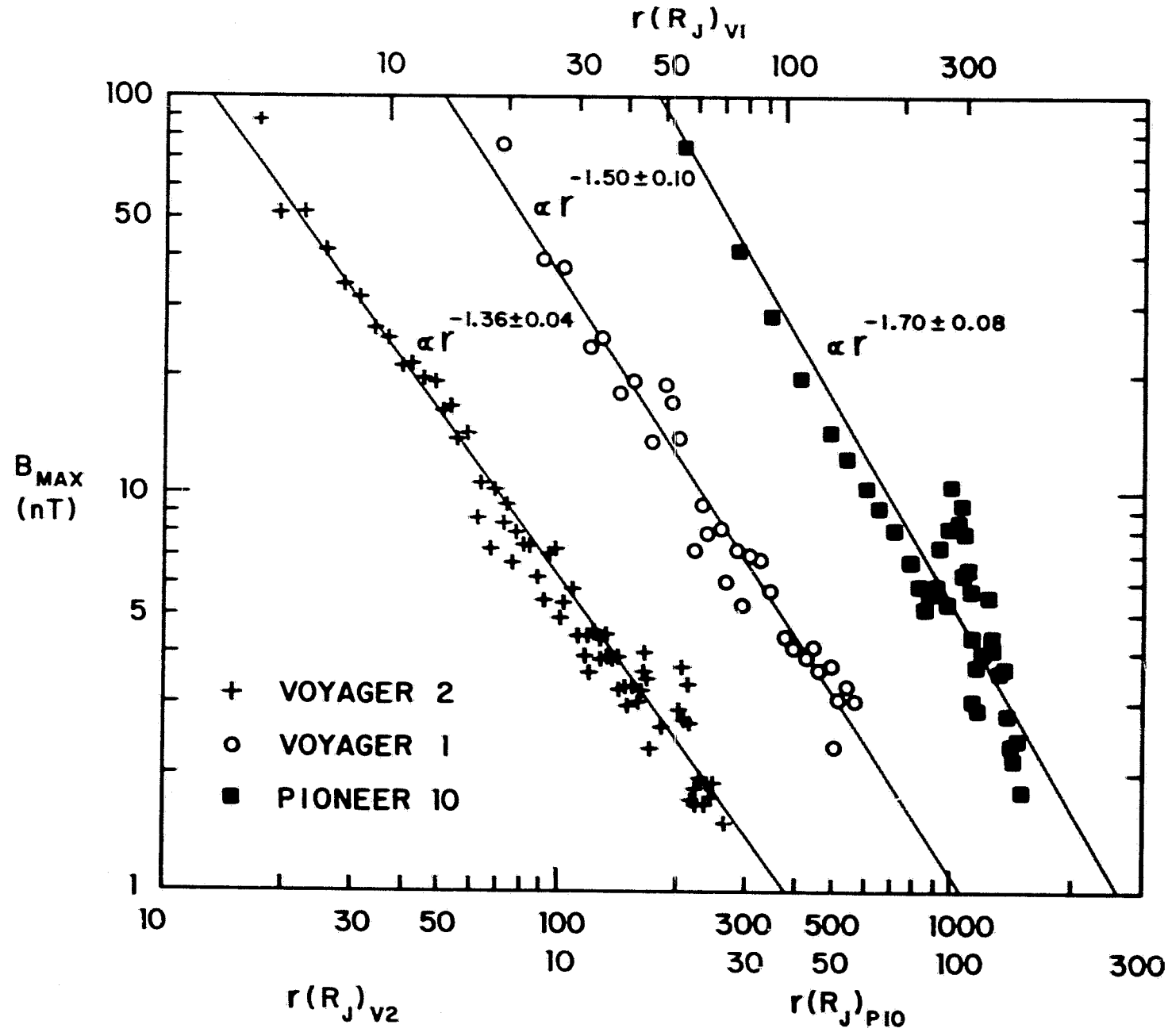
r(R_J)_V1
10
30
50
100
300
100
50
10
5
1
B_MAX (nT)
∝ r^-1.50±0.10
∝ r^-1.36±0.04
∝ r^-1.70±0.08
+ VOYAGER 2
o VOYAGER 1
■ PIONEER 10
10
30
50
100
300
500
1000
10
30
50
100
300
r(R_J)_V2
r(R_J)_P10

Figure 9

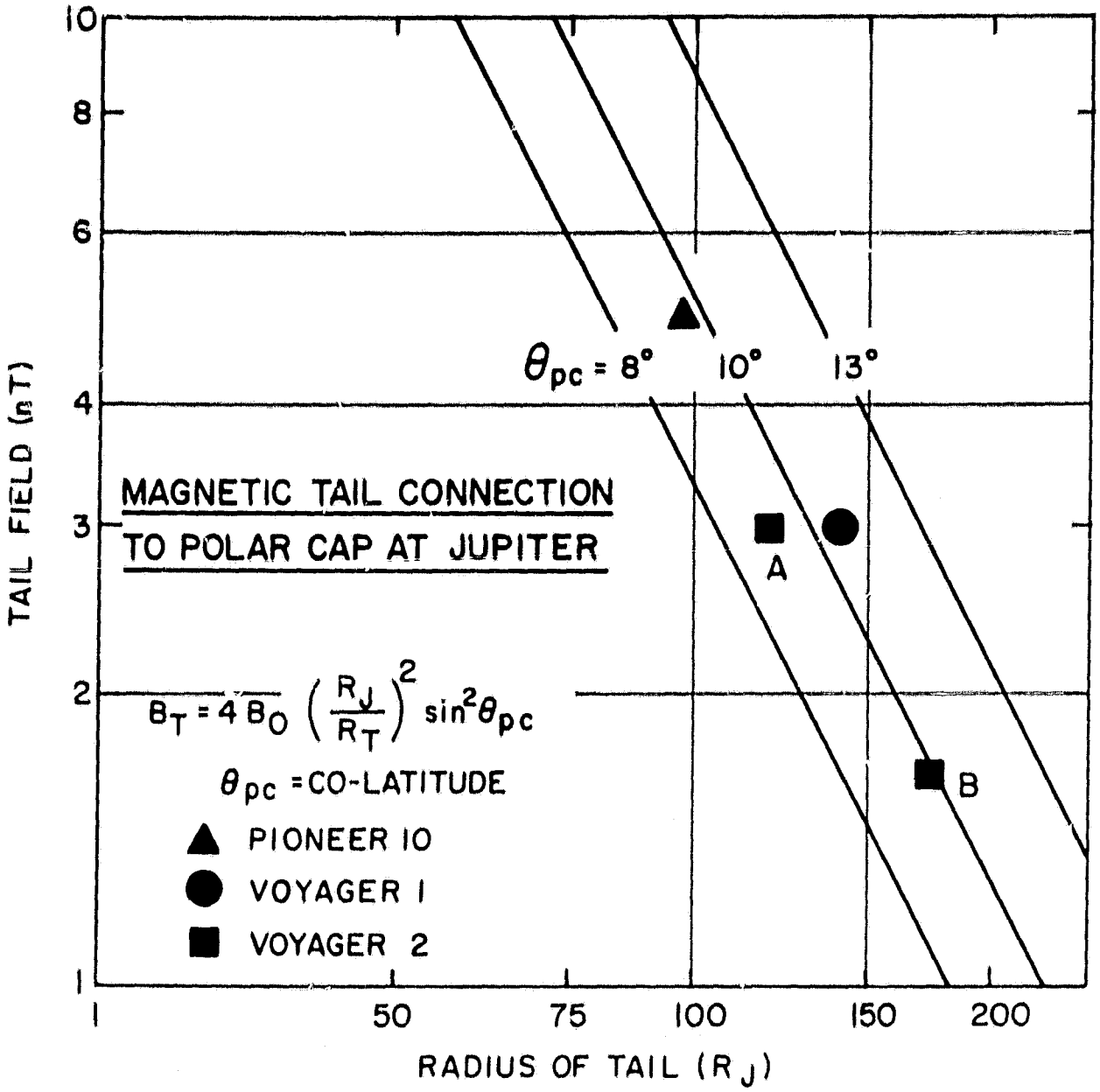
MAGNETIC TAIL CONNECTION
TO POLAR CAP AT JUPITER
$B_T = 4 B_O \left(\frac{R_J}{R_T}\right)^2 \sin^2\theta_{pc}$
θ_{pc} = CO-LATITUDE
PIONEER 10
VOYAGER 1
VOYAGER 2
θ_{pc} = 8°
10°
13°
A
B
TAIL FIELD (nT)
RADIUS OF TAIL (R_J)
10
8
6
4
3
2
1
1
50
75
100
150
200

Figure 10

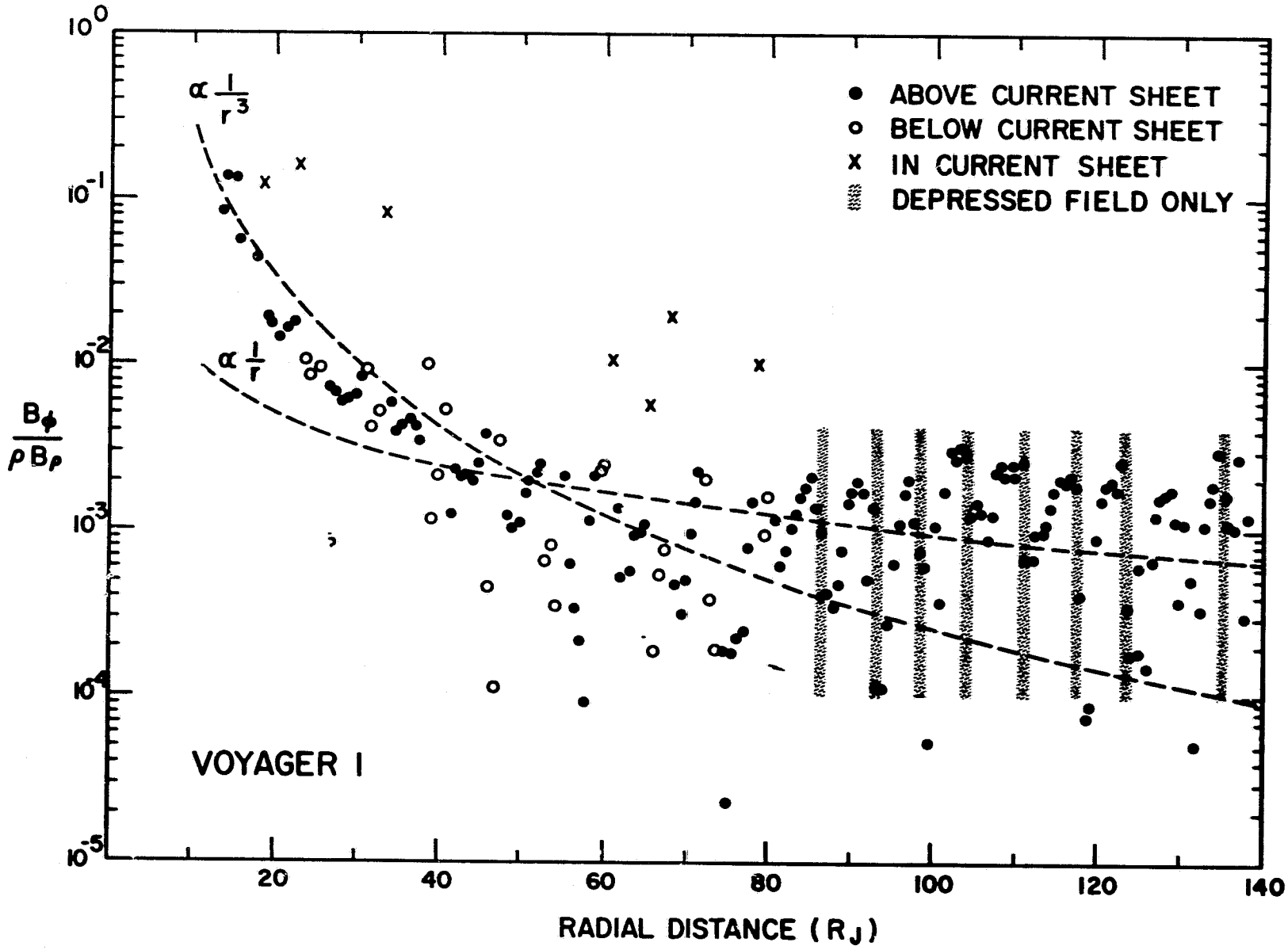
ABOVE CURRENT SHEET
BELOW CURRENT SHEET
IN CURRENT SHEET
DEPRESSED FIELD ONLY
$\propto \frac{1}{r^3}$
$\propto \frac{1}{r}$
VOYAGER I
$\frac{B_\phi}{\rho B_\rho}$
10^0
10^{-1}
10^{-2}
10^{-3}
10^{-4}
10^{-5}
20
40
60
80
100
120
140
RADIAL DISTANCE (R_J)

Figure 11

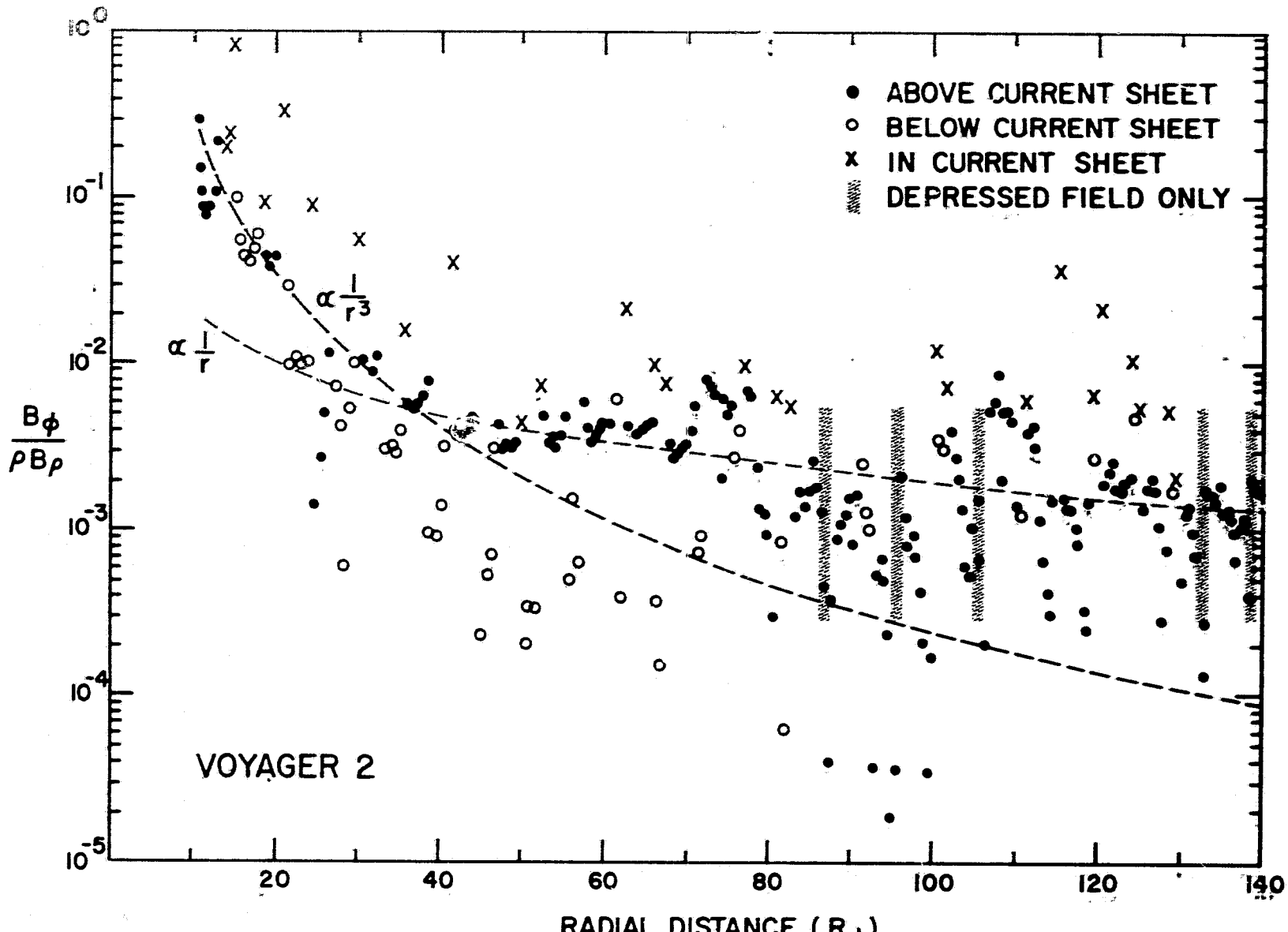
ABOVE CURRENT SHEET
BELOW CURRENT SHEET
IN CURRENT SHEET
DEPRESSED FIELD ONLY
VOYAGER 2
$\alpha \frac{1}{r^3}$
$\alpha \frac{1}{r}$
$\frac{B_\phi}{\rho B_\rho}$
10^0
10^{-1}
10^{-2}
10^{-3}
10^{-4}
10^{-5}
20
40
60
80
100
120
140
RADIAL DISTANCE (R_J)

Figure 12

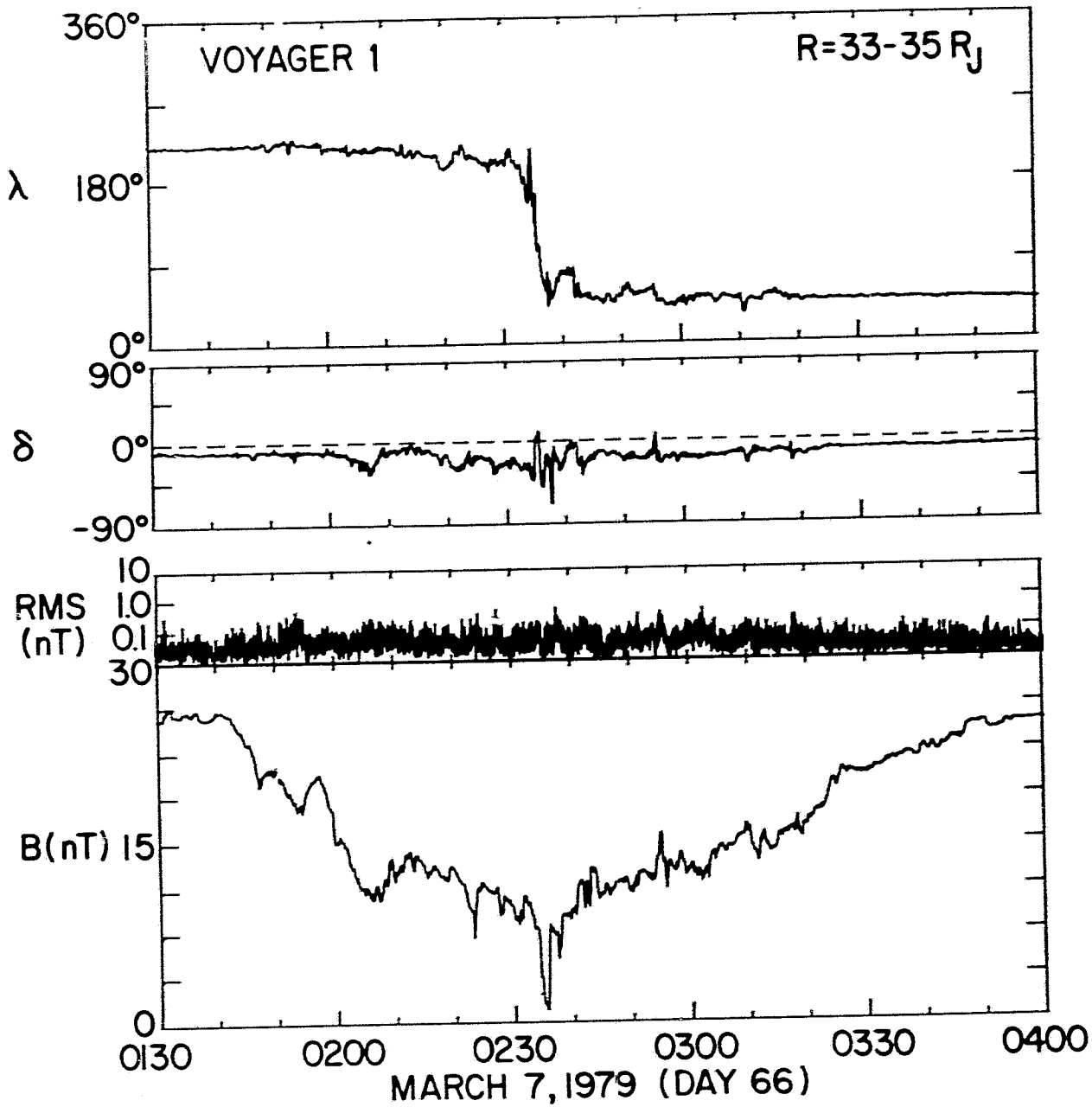
VOYAGER 1
R=33-35 R_J
360°
λ
180°
0°
90°
δ
0°
-90°
10
RMS
(nT)
1.0
0.1
30
B(nT) 15
0
0130
0200
0230
0300
0330
0400
MARCH 7, 1979 (DAY 66)

Figure 13

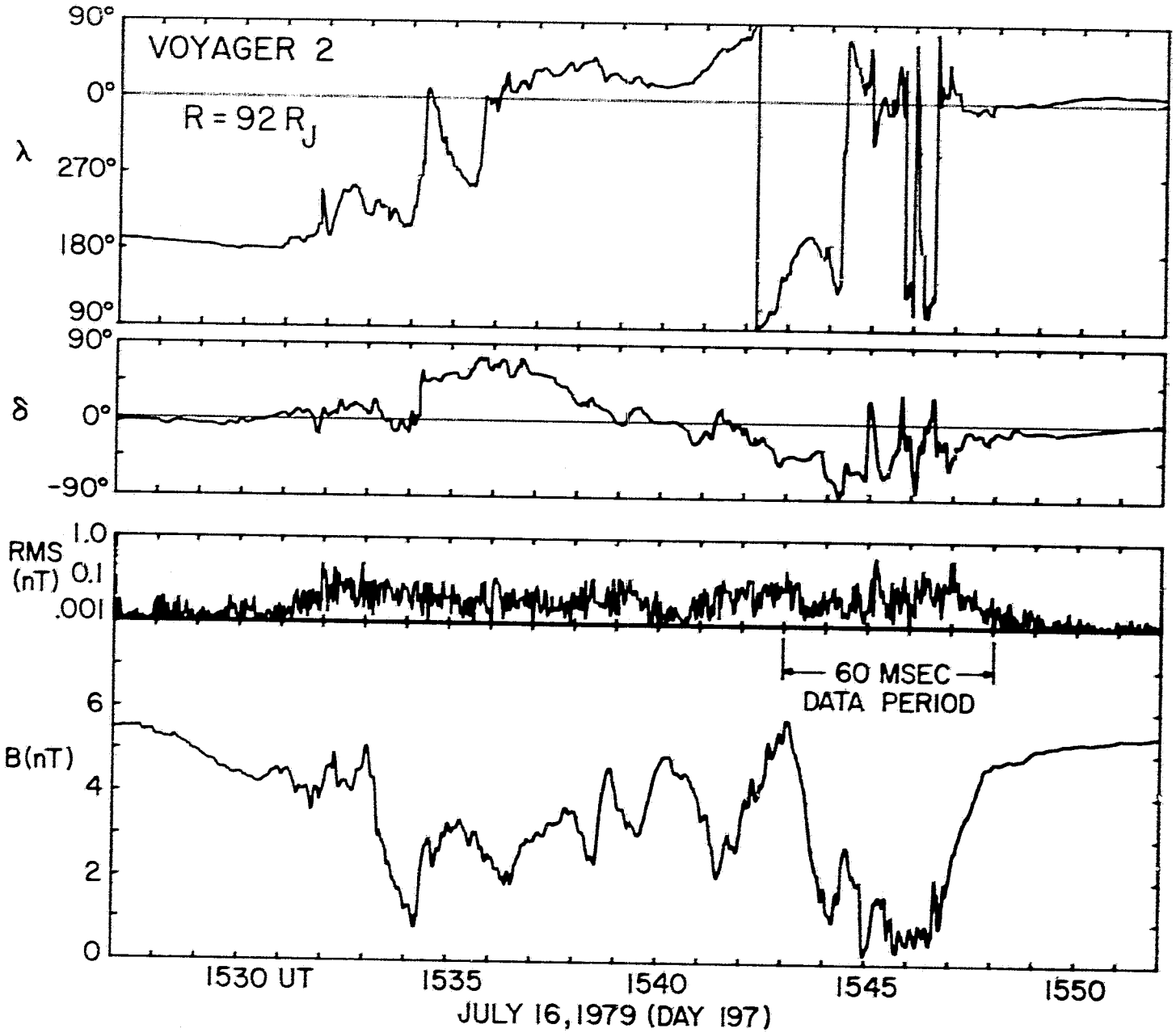
VOYAGER 2
R = 92 R_J
λ
90°
0°
270°
180°
90°
δ
90°
0°
-90°
RMS (nT)
1.0
0.1
.001
60 MSEC DATA PERIOD
B(nT)
6
4
2
0
1530 UT
1535
1540
1545
1550
JULY 16, 1979 (DAY 197)

Figure 14

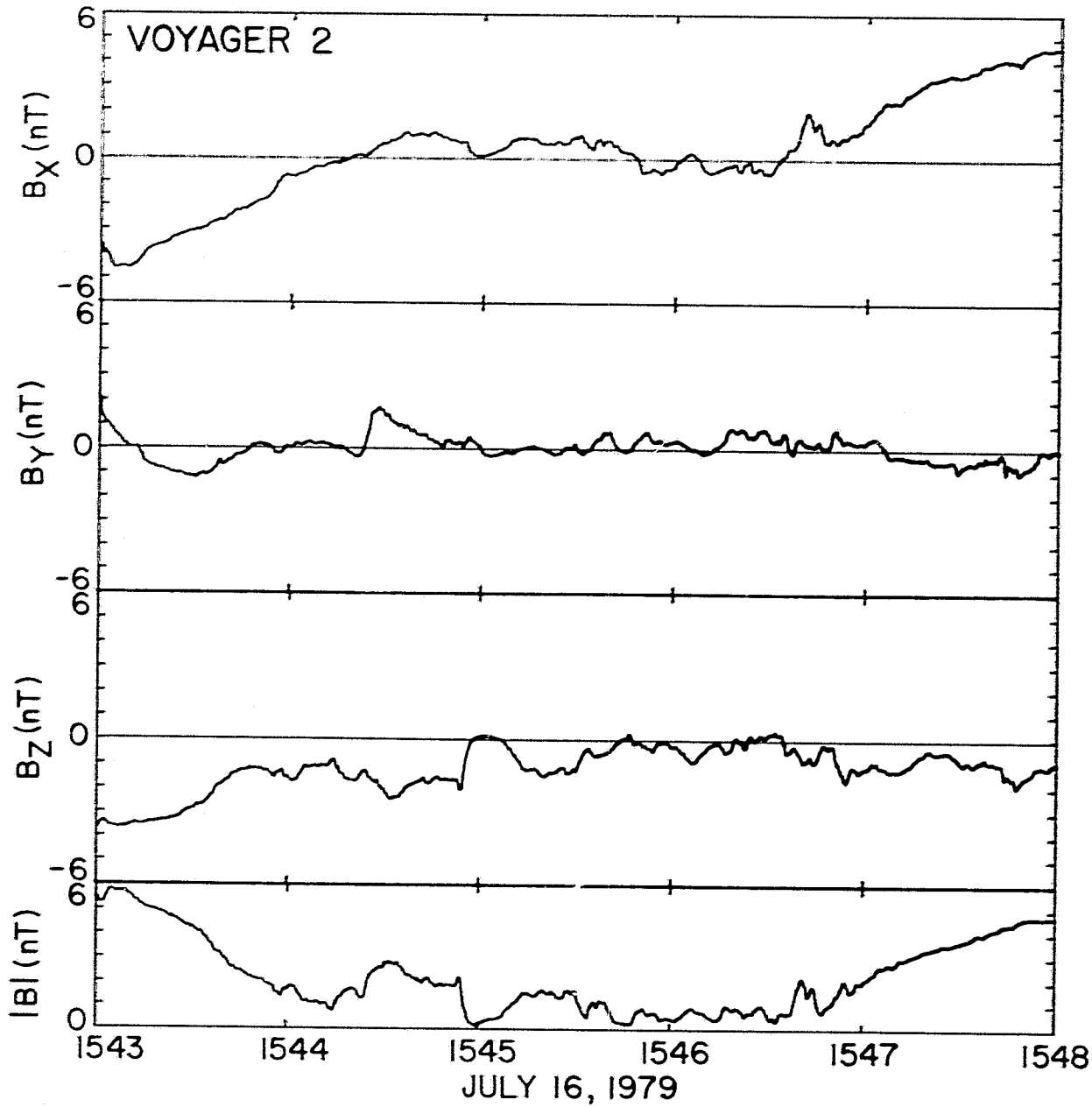
VOYAGER 2
B_X (nT)
B_Y (nT)
B_Z (nT)
|B| (nT)
6
0
-6
1543
1544
1545
1546
1547
1548
JULY 16, 1979

Figure 15

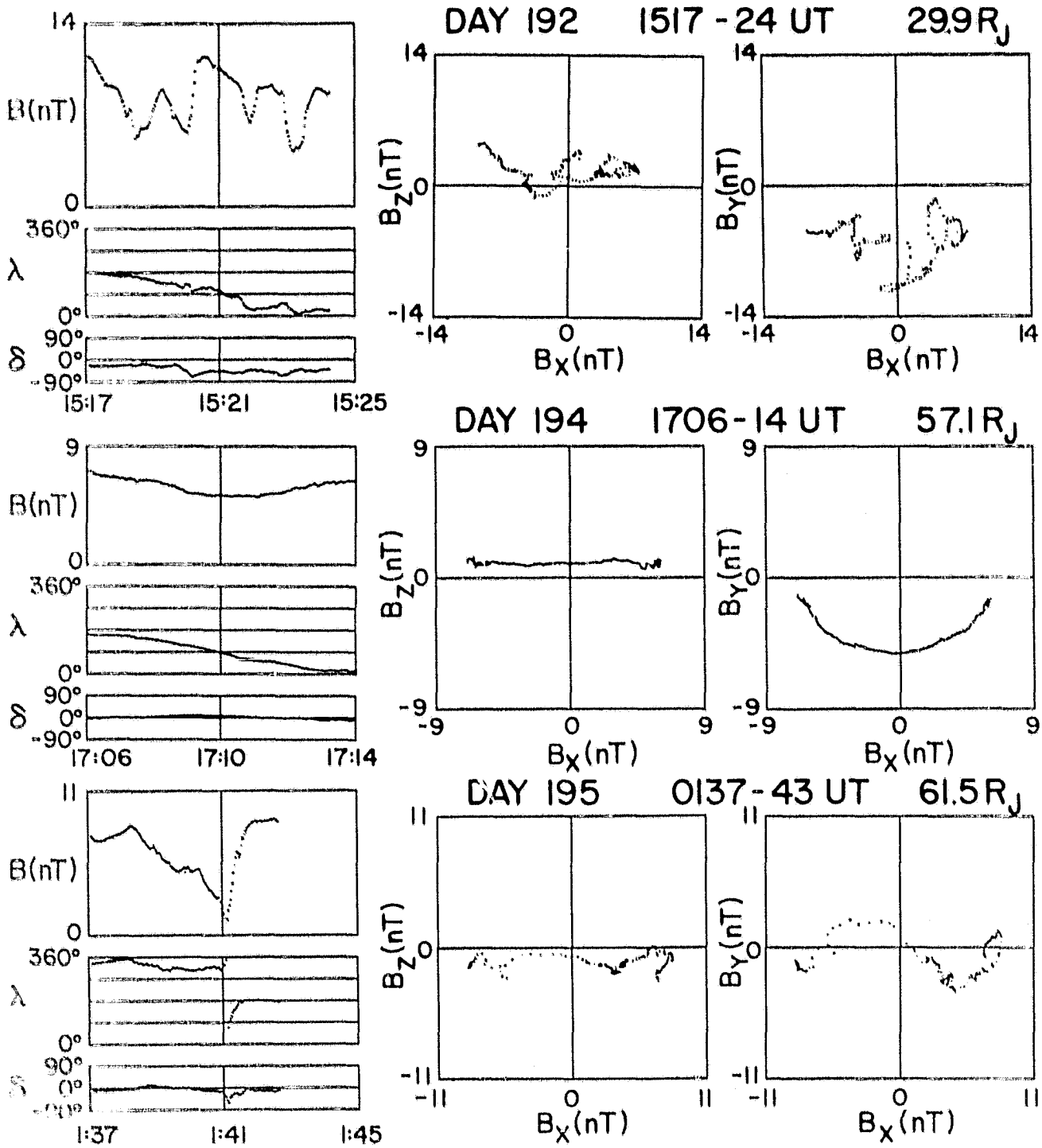
DAY 192 1517-24 UT 29.9 R_J
DAY 194 1706-14 UT 57.1 R_J
DAY 195 0137-43 UT 61.5 R_J
B(nT)
λ
δ
B_Z(nT)
B_Y(nT)
B_X(nT)
15:17
15:21
15:25
17:06
17:10
17:14
1:37
1:41
1:45

Figure 16

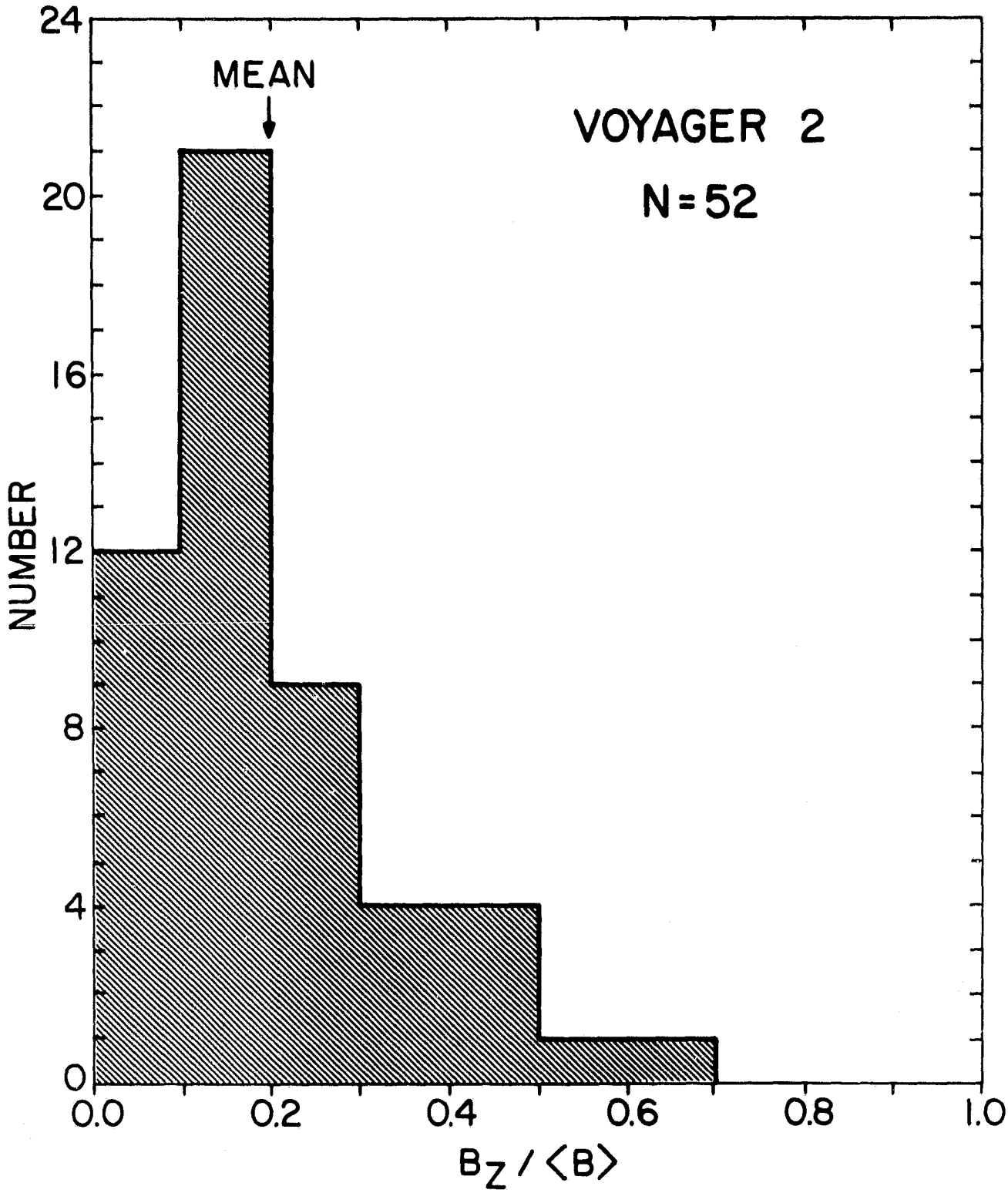
MEAN
VOYAGER 2
N=52
NUMBER
24
20
16
12
8
4
0
0.0
0.2
0.4
0.6
0.8
1.0
$B_Z / \langle B \rangle$

Figure 17

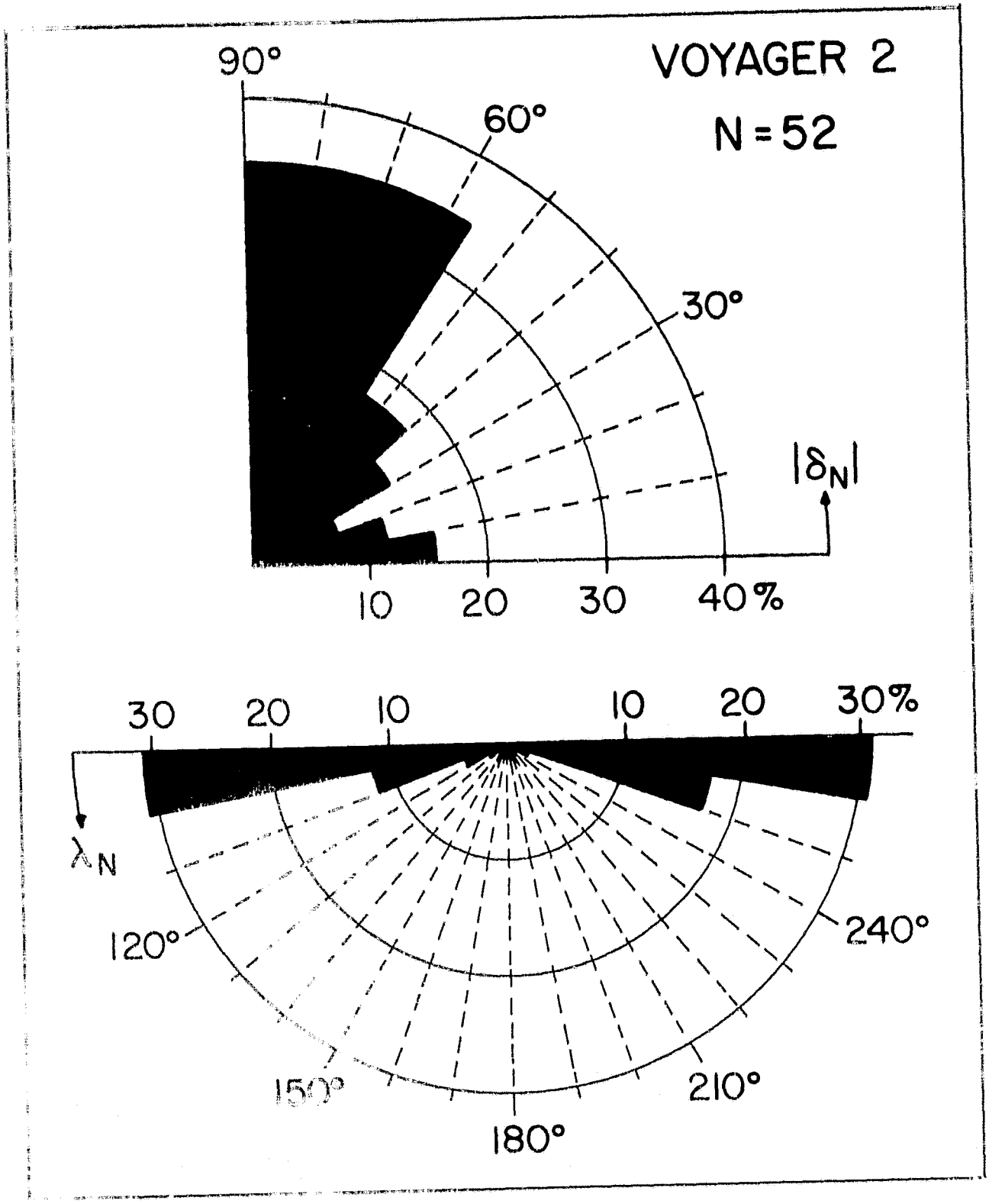

Figure 18

ORIGINAL PAGE IS
OF POOR QUALITY

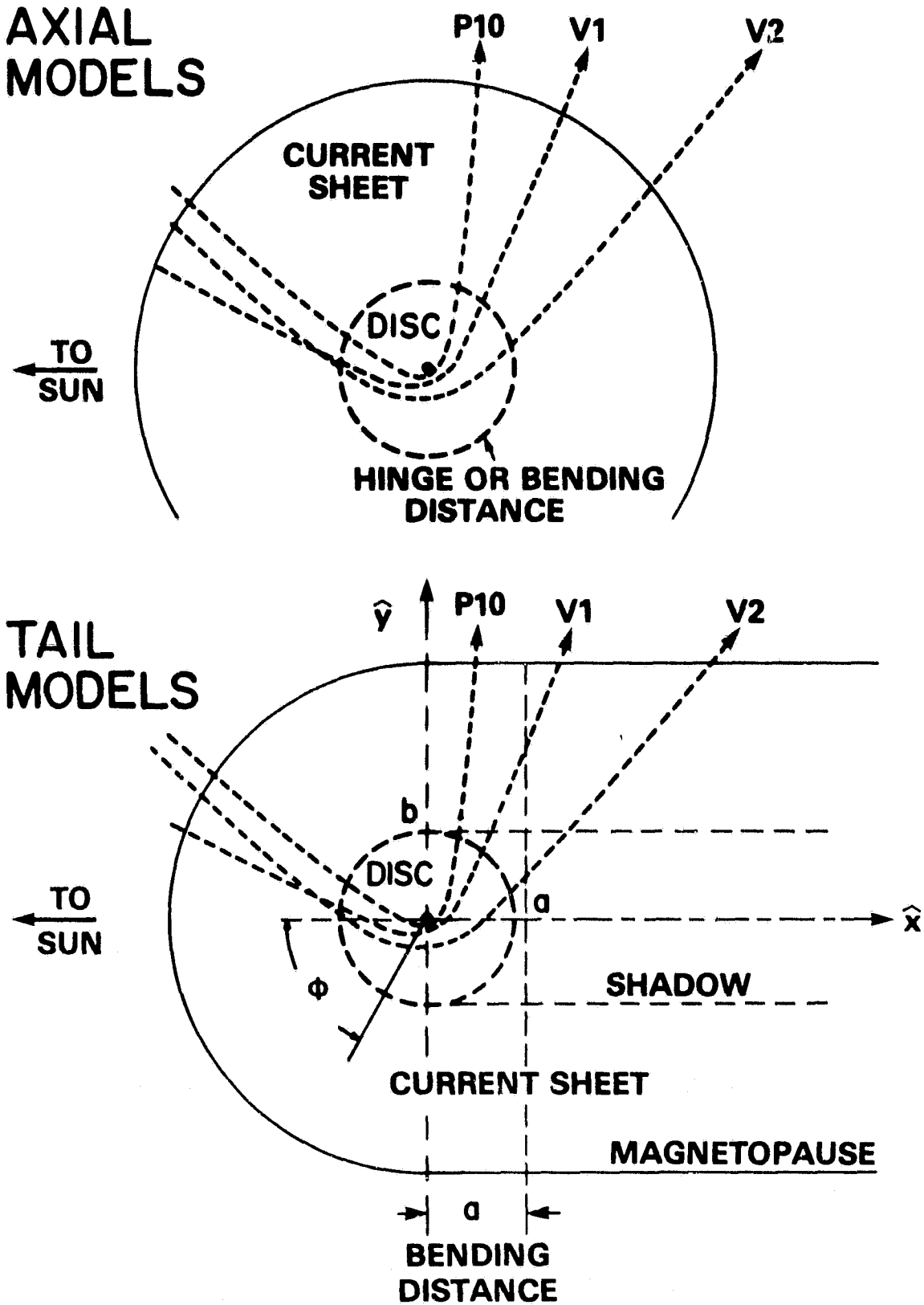
AXIAL MODELS
P10
V1
V2
CURRENT SHEET
DISC
TO SUN
HINGE OR BENDING DISTANCE
TAIL MODELS
ŷ
P10
V1
V2
b
DISC
a
x̂
TO SUN
Φ
SHADOW
CURRENT SHEET
MAGNETOPAUSE
a
BENDING DISTANCE

Figure 19

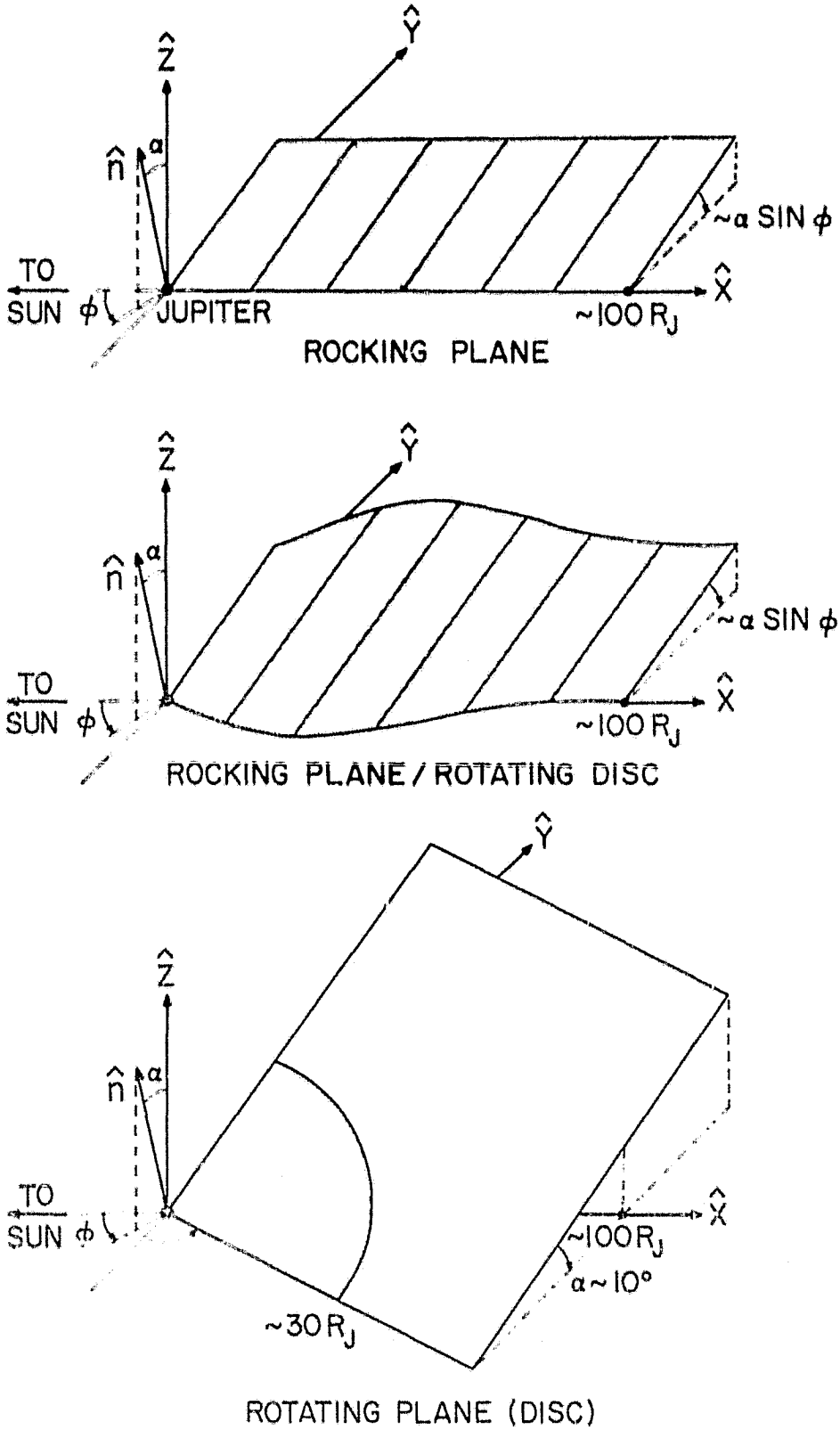
Ŷ
Ẑ
n̂
α
~α SIN φ
TO
SUN
φ
JUPITER
X̂
~100 R_J
ROCKING PLANE
Ŷ
Ẑ
n̂
α
~α SIN φ
TO
SUN
φ
X̂
~100 R_J
ROCKING PLANE / ROTATING DISC
Ŷ
Ẑ
n̂
α
TO
SUN
φ
X̂
~100 R_J
α ~ 10°
~30 R_J
ROTATING PLANE (DISC)

Figure 20

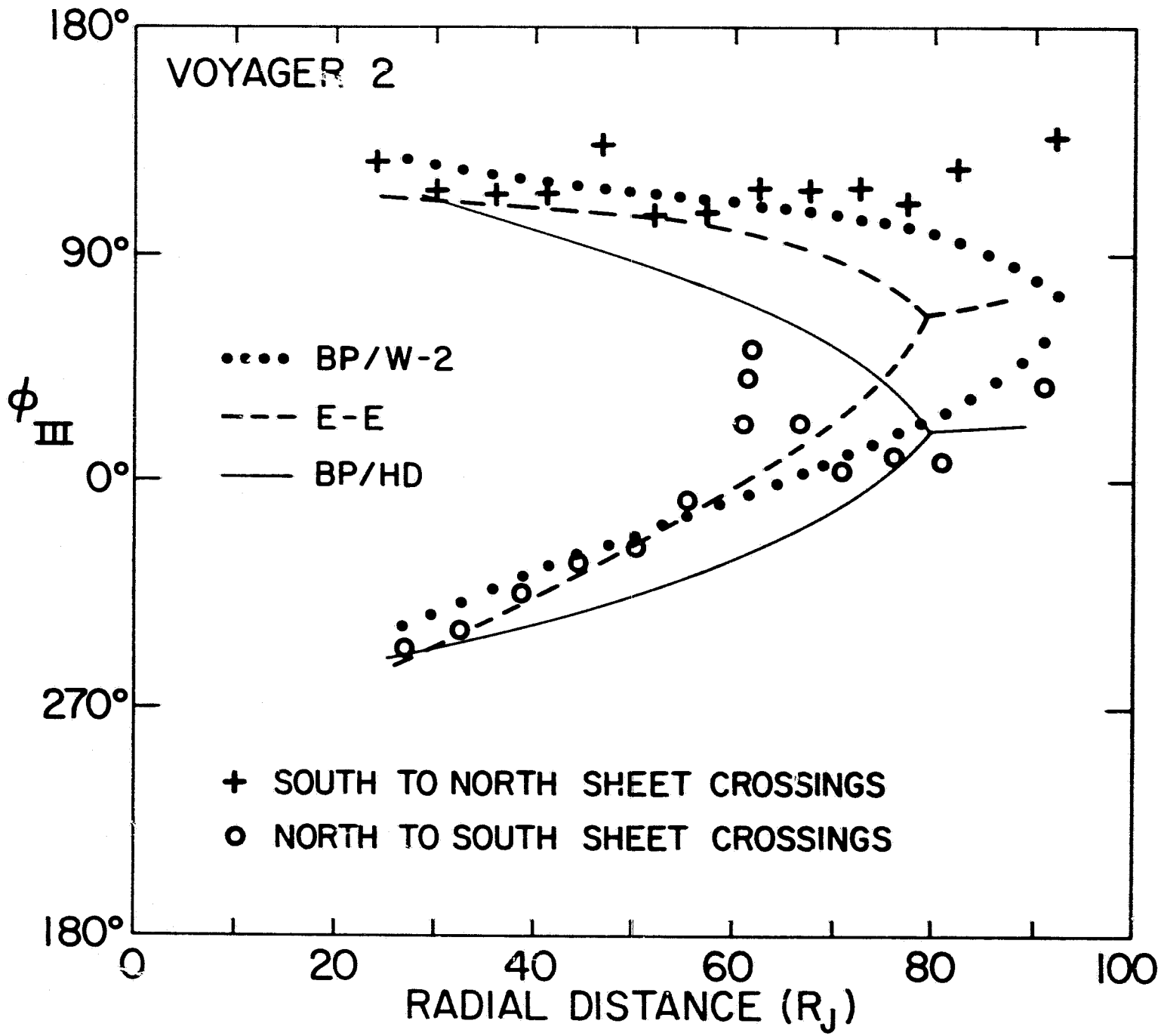
VOYAGER 2
BP/W-2
E-E
BP/HD
+ SOUTH TO NORTH SHEET CROSSINGS
o NORTH TO SOUTH SHEET CROSSINGS
ϕ_{III}
180°
90°
0°
270°
180°
0
20
40
60
80
100
RADIAL DISTANCE (R_J)

Figure 21

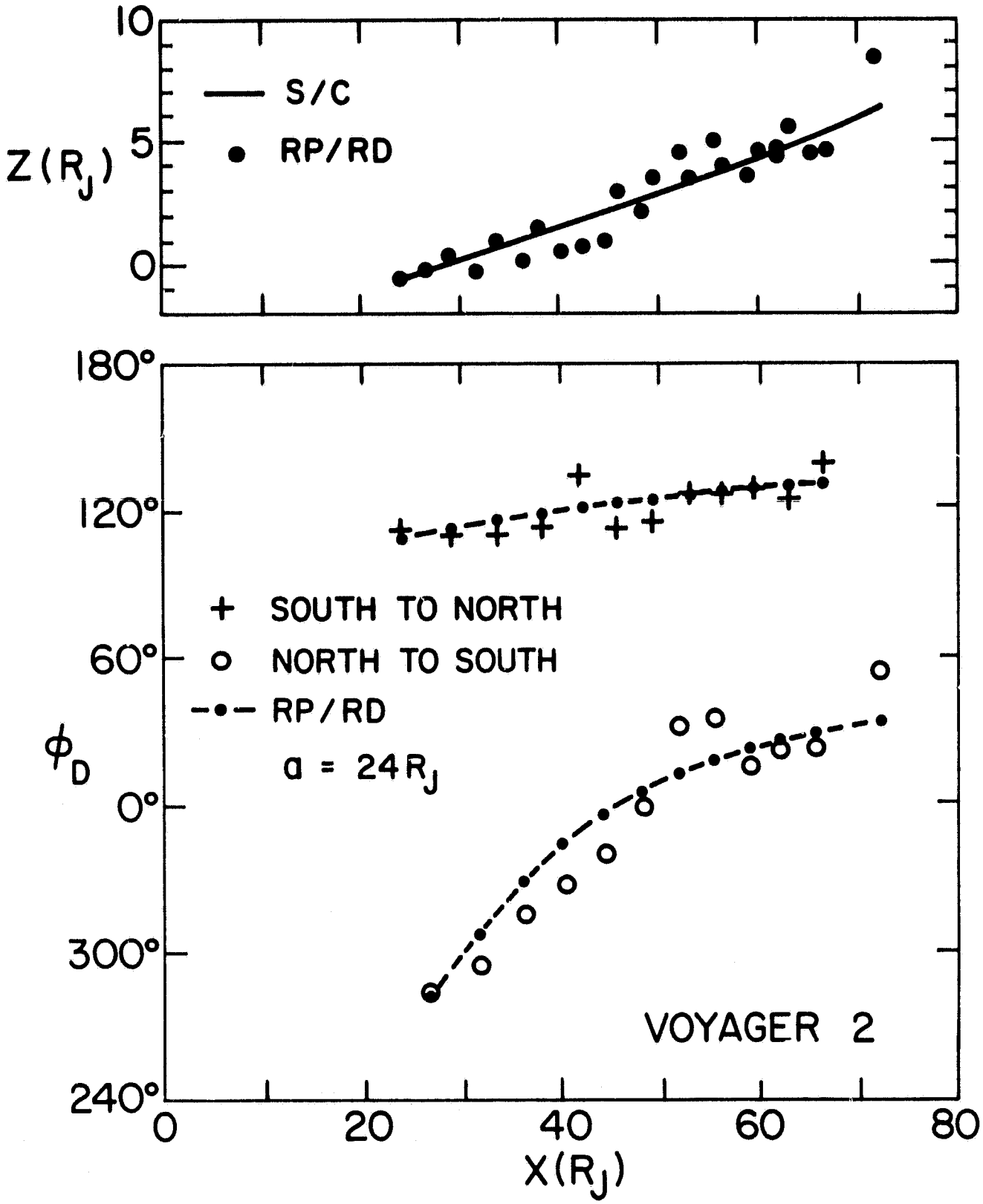
10
5
0
Z(R_J)
S/C
RP/RD
180°
120°
60°
0°
300°
240°
φ_D
+ SOUTH TO NORTH
o NORTH TO SOUTH
RP/RD
a = 24R_J
VOYAGER 2
0
20
40
60
80
X(R_J)

Figure 22

ABSTRACT

Analyses of Voyager magnetic field measurements have extended our understanding of the structural and temporal characteristics of Jupiter's magnetic tail. The magnitude of the magnetic field in the lobes of the tail is found to decrease with Jovicentric distance approximately as $r^{-1.4}$, compared with the power law exponent of -1.7 found for the rate of decrease along the Pioneer 10 outbound trajectory. Voyager observations of magnetic field component variations with Jovicentric distance in the tail do not support the uniform radial plasma out-flow model derived from Pioneer data. Voyager 2 has shown that the azimuthal current sheet which surrounds Jupiter in the inner and middle magnetosphere extends "tailward" (in the anti-Sun direction) to a distance of at least 100 R_J. In the tail this current sheet consists of a plasma sheet and embedded "neutral" sheet. In the region of the tail where the sheet is observed, the variation of the magnetic field as a result of the sheet structure and its 10-hr periodic motion is the dominant variation seen. Studies of both the large-scale configuration of the current sheet viewed as a surface and of the internal structure of the sheet and its orientation indicate that (1) at distances $\gtrsim$ 30 R_J in the tail the sheet is oriented within ±10° of the Jovian equatorial plane, most likely as a result of the solar wind interaction with the Jovian magnetosphere; (2) the surface moves north and south with an amplitude of several R_J with respect to that plane; and (3) at large distances this motion is primarily due to a rocking of the current sheet about the Jupiter-Sun line. A mathematical model that takes the tail geometry into account provides a simpler description of sheet motion in the deep tail than models based on axial symmetry. The plasma sheet in the tail is estimated to have an average thickness $\leq$ 5 R_J.